AN EXPERIMENTAL INVESTIGATION OF TRANSITION OF A PLANE POISEUILLE FLOW

Thesis for the Degree of Ph. D.
MICHIGAN STATE UNIVERSITY
MICHAEL ALLAN KARNITZ
1971

This is to certify that the

thesis entitled

AN EXPERIMENTAL INVESTIGATION OF TRANSITION OF A PLANE POISEUILLE FLOW

presented by

Michael Allan Karnitz

has been accepted towards fulfillment
of the requirements for

Ph.D. degree in **Mechanical Engineering**

Merle C. Potter M C Smith

Major professor

Date **May 20, 1971**

ABSTRACT

AN EXPERIMENTAL INVESTIGATION
OF TRANSITION OF A PLANE
POISEUILLE FLOW

By

Michael Allan Karnitz

The transition process of flow between parallel plates is investigated experimentally. The primary purpose is to relate the initial stage of the transition process to linear stability theory. To verify the critical Reynolds number predicted by linear theory a high aspect ratio channel (70 to 1) is employed, using air as the fluid.

The results indicate that as the velocity disturbance level in the channel is decreased, the transition Reynolds number monotonically increases. At the minimum disturbance level for this facility, a Reynolds number of 6, 700 is the largest attained for a laminar parabolic flow. This compares with a critical Reynolds number of 7, 700 predicted by linear stability theory.

Near the transition Reynolds number small regular waves near the walls are observed and considered to be Tollmein-Schlichting waves. These waves lead directly to a turbulent burst. When turbulence is observed in the channel it is in the form of a

mass of turbulent fluid, a turbulent slug, which is two-dimensional in nature.

AN EXPERIMENTAL INVESTIGATION OF TRANSITION OF A PLANE POISEUILLE FLOW

By

Michael Allan Karnitz

A THESIS

Submitted to
Michigan State University
in partial fulfillment of the requirements
for the degree of

DOCTOR OF PHILOSOPHY

Department of Mechanical Engineering

1971

ACKNOWLEDGMENTS

The author wishes to express his appreciation to Mr. Richard W. Jenkins for his valuable aid in construction of the facility. Appreciation is extended to his Major Professors: Dr. Merle C. Potter and Dr. Mahlon C. Smith for their valuable guidance throughout this study. The author's graduate work has been made possible through their patience, understanding and personal interest.

Thankful acknowledgment is also extended to Dr. Charles R. St. Clair, Jr., Chairman, Mechanical Engineering Department and to members of the Guidance Committee: Dr. James V. Beck, Dr. Robert H. Wasserman, and Dr. Carl M. Cooper.

The author is grateful for financial support received from a NDEA IV Fellowship and for supporting funds from the Mechanical Engineering Department and Division of Engineering Research.

The author dedicates this dissertation to his wife, Delores and his Mother, Marie.

TABLE OF CONTENTS

APPENDICES

LIST OF TABLES

LIST OF FIGURES

NOMENCLATURE

A	Cross-sectional area
$C = C_r + iC_i$	Complex propagation
C_i	Amplification factor
C_r	Wave speed
d_H	Hydraulic diameter
f	Frequency
h or d	Height
L	Length
P	Pressure
Pe	Perimeter
Rey or R	Reynolds number based on average velocity and channel height
t	Time
U	x-component of primary flow
u	x-component of velocity
u_i	Components of velocity
u'	Perturbation in x-component of velocity
V	Average velocity
v	y-component of velocity
w	Width

x, y, z	Coordinate axes
∇^2	Laplacian
α	Dimensionless wave number
λ^*	Wave length--dimensional
λ	Dimensionless wave length
ν	Kinematic viscosity
ϕ	Amplitude function
ρ	Density
τ	Shear stress
ψ	Stream function

CHAPTER I

INTRODUCTION

1.1 Literature Review

The transition process between laminar and turbulent flow has many different paths. The path which yields the simplest mathematical model, referred to as linear stability theory, involves an infinitesimal wave which grows, eventually leading to turbulence. Experimentally, to show that linear stability theory is valid, all extraneous effects which might cause a different route to transition must be suppressed.

The first study of transition from laminar to turbulent flow for a parallel shear flow was made by Osborne Reynolds (1883). He determined experimentally that the transition Reynolds number (based on average velocity and pipe diameter) in a round pipe occurs at approximately 2,000. The transition Reynolds number is referred to here and throughout this study as the experimental value at which the first sign of turbulence is observed. Reynolds hypothesized that the transition Reynolds number could be increased if care were taken to reduce the disturbances in the flow at the entrance of the pipe.

Reynolds also observed in a laminar pipe flow (with the use of dye) a small moving mass of turbulent fluid, referred to as a slug or burst. These turbulent slugs were further investigated by M. Couette (1890). He detected a regular oscillatory variation of the turbulent slugs which was caused by a variation in the mean flow.

One of the first studies conducted in a rectangular channel was made by S. J. Davies and C. M. White (1929). In their channel, transition occurred at a Reynolds number (based on average velocity and channel height) of 1, 400.

The theoretical work for Poiseuille flow between parallel plates was studied by many investigators, one being C. C. Lin (1945). He presented the most conclusive study in which he used linear theory (disturbance waves with infinitesimal amplitudes). Working with asymptotic methods, he obtained a critical Reynolds number (based on average velocity and channel height) of 7, 100. The critical Reynolds number is the theoretical value at which a wave starts to grow. Lin also gave the asymptotic theory a firm mathematical footing by explaining the behavior of the functions near the singularities. Lin's work was verified by L. H. Thomas (1953) by using a numerical method. The Reynolds number of 7, 700, calculated by Thomas, is the more accurate value.

The initial verification of linear stability theory for a flat plate boundary layer was done by G. B. Schubauer and H. K. Skramstad (1947). They induced oscillation in a laminar boundary

layer and observed the small sinusoidal waves, Tollmein-Schlichting waves, predicted by linear theory. The latter stages of transition of a flat plate boundary layer were thoroughly examined by H. W. Emmons (1951) and G. B. Schubauer and P. S. Klebanoff (1956). They noted that amplified waves became turbulent spots which moved downstream growing steadily in all directions.

Further work on turbulent bursts in a rectangular channel was renewed by G. C. Sherlin (1960). He determined the growth and propagation speed of turbulent slugs in a rectangular duct (using water) with a channel aspect ratio of 4. The turbulence was induced by injecting dye and the Reynolds numbers (based on average velocity and half the hydraulic diameter - $d_H = 4A/Pe$) were in the range of 600-2, 100. Sherlin's study of the growth of turbulent slugs was extended by M.A.B. Narayanan and T. Narayana (1968). They determined that the intermittency increased with increasing downstream positions at various Reynolds numbers. Their natural transition, for a channel aspect ratio of 12, occurred at a Reynolds number of 3, 000. Natural transition is defined as transition without the introduction of artificial disturbances.

A theoretical stability analysis was performed by W. C. Reynolds and M. C. Potter (1967) for a wave of finite amplitude in a parallel shear flow. They concluded that a relatively weak but finite disturbance markedly reduced the critical Reynolds number and suggested that a 2. 5% disturbance intensity level, defined by

eq. (2.17), could reduce the critical Reynolds number from 7,700 to 1,400. It must be realized that the analysis predicts only the initial stage of transition.

Mean velocity profiles and skin friction in air were measured by V. C. Patel and M. R. Head (1969) with a channel aspect ratio of 48. They were interested in obtaining a precise definition of the term "fully developed turbulent flow". Their critical Reynolds number (based on average velocity and channel height) for transition, where the first bursts appeared, was about 2,000.

More recently John A. Breslin (1970) has experimentally looked further into the bursting phenomenon in air with a channel aspect ratio of 10. His turbulent slugs were artificially introduced with a puffer device and his critical Reynolds number (based on average velocity and half the hydraulic diameter) for natural transition was approximately 2,500. He proposed that there is flow away from the wall in front of a slug and this makes the laminar flow less stable by making it easier for flow reversal and separation to occur near the wall, while at the rear of the slug there is flow toward the wall which tends to suppress flow separation.

1.2 Description of the Problem

The primary purpose of the present study is to examine the transition process of a plane Poiseuille flow subject to small disturbances, that is, to experimentally examine linear stability theory. A high aspect ratio channel is used to guarantee a two-dimensional

flow. Previous transition studies for a plane Poiseuille flow have been conducted in channels where the transition Reynolds numbers (based on average velocity and channel height) were 3,000 or less. In relating linear stability theory with experimental work the Reynolds number must be raised considerably above the 3,000 value of previous investigations; hence, it is necessary to substantially reduce the disturbance level which naturally exists in a channel flow. It is assumed that it is experimentally impossible to attain a higher Reynolds number than the minimum value of 7,700 on the linear neutral stability loop, since linear theory implies growth of a zero-amplitude disturbance wave at that Reynolds number.

The linear theory also suggests that waves with various wave numbers become unstable and amplify at various Reynolds numbers. For example, at a dimensionless wave number ($\frac{2\pi h}{\lambda^*}$; h-channel height and λ^*-wave length) of 2.1 an infinitesimal wave is amplified at a Reynolds number of 7,700, yet for a wave number of 1.0 the Reynolds number increases to 12,000 before growth occurs. Artificially excited disturbances with controlled frequencies are introduced into the flow in this study so that the effect of the wave number can be noted.

Linear theory also predicts a two-dimensional transition process, which is, of course, inherent in the two-dimensional theory. In boundary layer transition it is observed experimentally that the transition process is a three-dimensional phenomenon.

Another objective of this study is to investigate the nature of the actual breakup of the waves in the transition process.

Finally, the turbulent slug, which is described by the investigators mentioned in section 1.1, is studied in further detail and its role in the natural transition process is examined.

CHAPTER II

STABILITY THEORY FOR PARALLEL SHEAR FLOWS

Results of stability theory are referred to throughout this work; hence, the general development will be presented here. The stability theory will be formulated for the case of an incompressible fluid. It will be assumed that a two-dimensional disturbance is more unstable than a three-dimensional disturbance which follows from Squire's (1933) analysis.

The basic dimensionless equations that must be satisfied are continuity

$$\frac{\partial u_i}{\partial x_i} = 0 \tag{2.1}$$

and momentum

$$\frac{\partial u_i}{\partial t} + u_j \frac{\partial u_i}{\partial x_j} = -\frac{\partial p}{\partial x_i} + \frac{1}{R} \nabla^2 u_i \tag{2.2}$$

where $\nabla^2 = \frac{\partial^2}{\partial x_1^2} + \frac{\partial^2}{\partial x_2^2}$, $\qquad R = \frac{u_{avg}\, d}{\nu}$

and d is the distance between the parallel plates. The pressure is eliminated from equations (2.2) by cross-differentiating and subtracting and with the introduction of the stream function there results

$$\frac{\partial}{\partial t}(\nabla^2\psi) + u\frac{\partial}{\partial x}(\nabla^2\psi) + v\frac{\partial}{\partial y}(\nabla^2\psi) - \frac{1}{R}\nabla^2(\nabla^2\psi) = 0 \qquad (2.3)$$

having used $u = \frac{\partial\psi}{\partial y}$ and $v = -\frac{\partial\psi}{\partial x}$.

To study disturbances, the stream function ψ is expanded in terms of a small parameter ϵ, which may be related to the amplitude of the disturbance, as follows:

$$\psi = \sum_{n=0}^{\infty} \epsilon^n \psi^{(n)} = \psi^{(0)} + \epsilon\psi^{(1)} + \epsilon^2\psi^{(2)} + \ldots \qquad (2.4)$$

The first term in the expansion $\psi^{(0)}$ is the stream function of the undisturbed primary flow and $\epsilon\psi^{(1)}$ is the first order perturbation of the stream function ψ.

The Laplacian of the stream function and the velocities are developed in terms of stream function expansions:

$$\nabla^2\psi = \nabla^2\left[\sum_{n=0}^{\infty} \epsilon^n \psi^{(n)}\right] = \sum_{n=0}^{\infty} \epsilon^n \nabla^2\psi^{(n)} \qquad (2.5)$$

$$u = \sum_{n=0}^{\infty} \epsilon^n \frac{\partial\psi^{(n)}}{\partial y} \qquad (2.6)$$

and

$$-v = \sum_{n=0}^{\infty} \epsilon^n \frac{\partial\psi^{(n)}}{\partial x} \qquad (2.7)$$

Substituting the above into eq. (2.3) yields

$$\sum_{n=0}^{\infty} \epsilon^n \frac{\partial}{\partial t}\nabla^2\psi^{(n)} + \sum_{p=0}^{\infty}\sum_{m=0}^{\infty} \epsilon^{p+m} \frac{\partial\psi^{(p)}}{\partial y}\frac{\partial\nabla^2\psi^{(m)}}{\partial x}$$

$$- \sum_{p=0}^{\infty}\sum_{m=0}^{\infty} \epsilon^{p+m} \frac{\partial\psi^{(p)}}{\partial x}\frac{\partial\nabla^2\psi^{(m)}}{\partial y} - \sum_{n=0}^{\infty} \epsilon^n \frac{1}{R}\nabla^2(\nabla^2\psi^{(n)}) = 0 \qquad (2.8)$$

Let m + p = n, then

$$\sum_{n=0}^{\infty} \epsilon^n \left[\frac{\partial}{\partial t} \nabla^2 \psi^{(n)} + \sum_{m=0}^{n} \frac{\partial \psi^{(n-m)}}{\partial y} \frac{\partial \nabla^2 \psi^{m}}{\partial x} \right.$$

$$\left. - \sum_{m=0}^{n} \frac{\partial \psi^{(n-m)}}{\partial x} \frac{\partial \nabla^2 \psi^{(m)}}{\partial y} - \frac{1}{R} \nabla^2 (\nabla^2 \psi^{(n)}) \right] = 0 \qquad (2.9)$$

where $n - m \geq 0$.

The coefficient of each ϵ term must be zero; hence,

$$\frac{\partial}{\partial t} \nabla^2 \psi^{(n)} + \sum_{m=0}^{n} \frac{\partial \psi^{(n-m)}}{\partial y} \frac{\partial \nabla^2 \psi^{(m)}}{\partial x} - \sum_{m=0}^{n} \frac{\partial \psi^{(n-m)}}{\partial x} \frac{\partial \nabla^2 \psi^{(m)}}{\partial y}$$

$$- \frac{1}{R} \nabla^2 (\nabla^2 \psi^{(n)}) = 0 \qquad (2.10)$$

The steady zeroeth order problem, n = m = 0, yields

$$\nabla^2 (\nabla^2 \psi^{(0)}) = 0 \qquad (2.11)$$

The solution of eq. (2.11) yields the primary velocity distribution. For flow between parallel plates, this would give a parabolic distribution for u(y) with v = 0.

The first order problem, n = 1 and m = 0 & 1, represents the linear stability problem or stability due to infinitesimal disturbances. The resulting equation is

$$\frac{\partial}{\partial t} \nabla^2 \psi^{(1)} + \frac{\partial \psi^{(1)}}{\partial y} \frac{\partial \nabla^2 \psi^{(0)}}{\partial x} + \frac{\partial \psi^{(0)}}{\partial y} \frac{\partial \nabla^2 \psi^{(1)}}{\partial x} - \frac{\partial \psi^{(1)}}{\partial x} \frac{\partial \nabla^2 \psi^{(0)}}{\partial y}$$

$$- \frac{\partial \psi^{(0)}}{\partial x} \frac{\partial \nabla^2 \psi^{(1)}}{\partial y} - \frac{1}{R} \nabla^2 (\nabla^2 \psi^{(1)}) = 0 \qquad (2.12)$$

which reduces, for a parallel shear flow, to

$$\frac{\partial}{\partial t}\nabla^2\psi^{(1)} + \frac{\partial\psi^{(0)}}{\partial y}\frac{\partial\nabla^2\psi^{(1)}}{\partial x} - \frac{\partial\psi^{(1)}}{\partial x}\frac{\partial\nabla^2\psi^{(0)}}{\partial y}$$

$$-\frac{1}{R}\nabla^2(\nabla^2\psi^{(1)}) = 0 \qquad (2.13)$$

since $\psi^{(0)} = \psi^{(0)}(y)$.

With the no-slip boundary conditions $\frac{\partial\psi^{(1)}}{\partial y} = \frac{\partial\psi^{(1)}}{\partial x} = 0$ at the two walls, $y = 0$ and 1.

The differential equation for $\psi^{(1)}$ is linear and has coefficients independent of x and t. On this basis, attempting a solution by separation of variables, one assumes periodicity in time and displacement as

$$\psi^{(1)} = \phi(y)\, e^{i\alpha x}\, e^{-i\alpha ct} \qquad (2.14)$$

where α, the dimensionless wave number, is real and $C = C_r + iC_i$, C_r is the wave speed and C_i is the growth or decay rate. The dimensionless wave length of the disturbance is $\lambda = \frac{2\pi}{\alpha}$. If C_i equals zero the wave neither grows nor decays so neutral stability results. Now, substituting eq. (2.14) into eq. (2.13) the resulting differential equation is

$$(U - C)(\phi'' - \alpha^2\phi) - U''\phi = \frac{1}{\alpha R}(\phi'''' - 2\alpha\phi'' + \alpha^4\phi) \qquad (2.15)$$

which is the famous Orr-Sommerfeld equation. The boundary conditions are the no-slip conditions and impermeability at both walls

$$\phi = \phi' = 0 \quad \text{at} \quad y = 0, 1\,. \qquad (2.16)$$

The solution of the Orr-Sommerfeld equation has been achieved by many investigators; the most comprehensive study was made by

C. C. Lin (1945). The primary results of interest are presented in a plot of wave number versus Reynolds number, shown in Figure 2.1. The neutral stability curve has a minimum Reynolds number usually referred to as the critical Reynolds number, of 7,700 at a wave number of 2.04. For the present channel with a height of 1/2 inch, this dimensionless wave number corresponds to a frequency of 86.5 hertz.

The Orr-Sommerfeld equation is a linear differential equation that was derived using the first order perturbation of the velocity field. For it to predict the growth of disturbances, the disturbances must be very small, usually referred to as infinitesimal.

The nonlinear theory employs higher order terms of the expansion of eq. (2.4). Using eq. (2.10), for $n > 1$, additional equations are introduced which account for finite disturbances.

Reynolds and Potter (1967), using a finite amplitude wave, solved eq. (2.10) for $n = 2$ and concluded that a finite disturbance shifted the neutral stability loop up and to the left as shown in Figure 2.1. They determined that a wave with 2.5% intensity could be responsible for reducing the critical Reynolds number from 7,700 to 1,400. The intensity is defined as

$$\% \text{ intensity} = \frac{\sqrt{\overline{u'^2}}}{U} \times 100 \qquad (2.17)$$

where u' is the disturbance function. In the linear theory it would be given by $\epsilon\psi^{(1)}$ and in the second order theory by $\left[\epsilon\psi^{(1)} + \epsilon^2\psi^{(2)}\right]$.

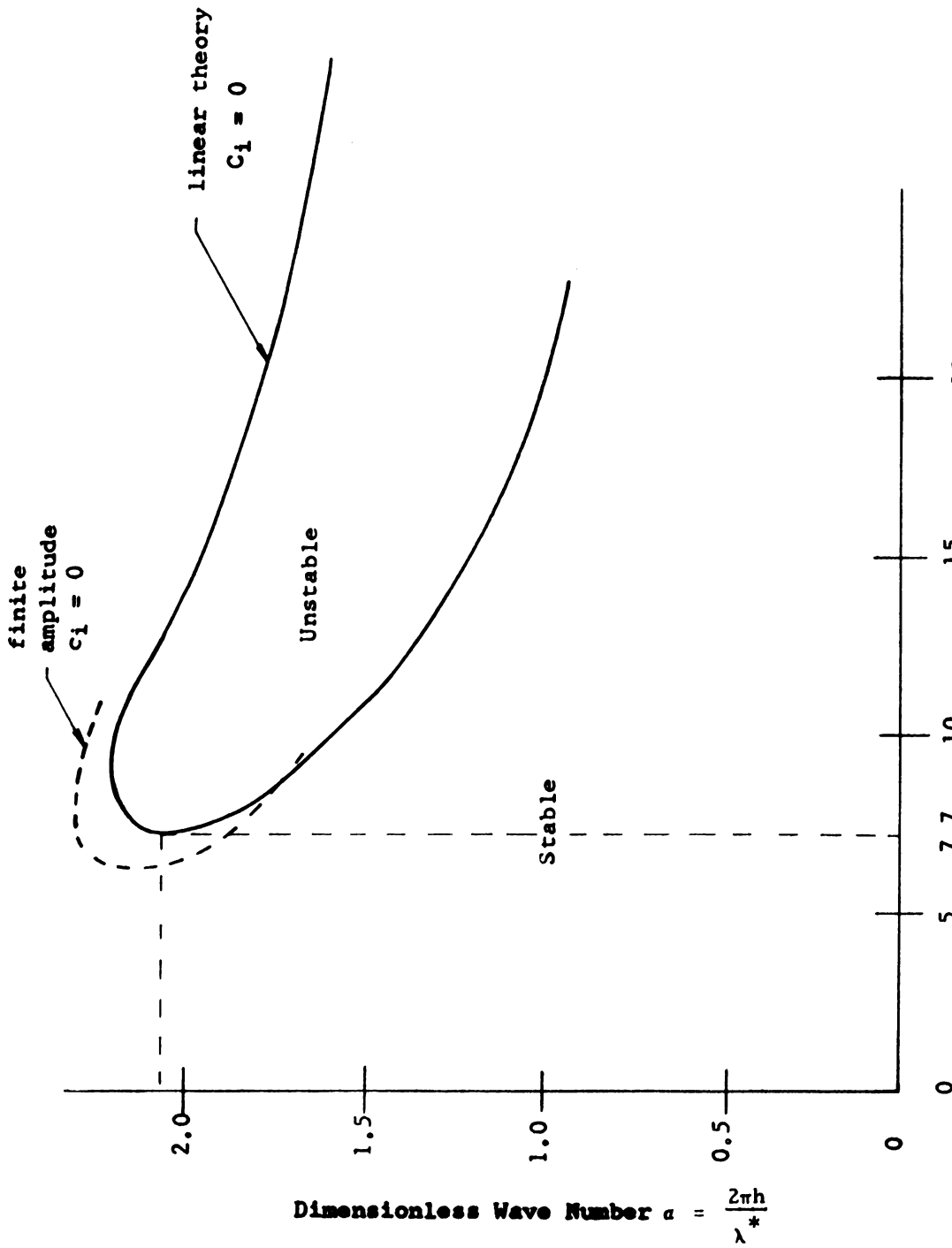

Figure 2.1 Stability Loops for a Plane Poiseuille Flow

Experimentally, the intensity in eq. (2.17) is measured by the use of a time averaging process on the u' hot-wire output signal. One phase of the experiment is to control the disturbance intensity and observe the relationship between the disturbance intensity and the transition Reynolds number. The value of 7,700 should be approached as the intensity is decreased in magnitude.

It can also be observed from the neutral stability curve in Figure 2.1 that disturbances with wave numbers near 2.0 lead to disturbance growth (instability) at Reynolds numbers near the critical value; however, disturbances with wave numbers either larger or smaller than this value lead to instability at larger Reynolds numbers.

The neutral stability curve in Figure 2.1 is only applicable for a parabolic velocity distribution. In the entrance region of the channel the velocity distribution is not parabolic and hence the stability characteristics are different from those of Figure 2.1. In an analytical investigation, T. E. Chen and E. M. Sparrow (1967) concluded that the entrance flow is more stable than the parabolic channel flow. Thus, it is anticipated that disturbances should grow to turbulence downstream of the entrance region.

Finally, the disturbances investigated analytically are all assumed to be two-dimensional. An interesting question is the possibility of the growth of a disturbance into turbulence while

maintaining its initial two-dimensionality as compared to the three-dimensional break-up phenomenon, as observed experimentally in a boundary layer.

CHAPTER III

EXPERIMENTAL APPARATUS

3.1 Flow System

The channel built for the present investigation, using air as the fluid, is 24 feet long, 35 inches wide and 1/2 inch high, thus having an aspect ratio of 70. The entrance region of the test section consists of a settling chamber, approximately 1 foot by 3 feet in cross-section and 5 feet long, and a streamlined contraction from 1 foot to 1/2 inch in a 6 foot long section. At the end of the channel there is a plenum chamber evacuated by a centrifugal blower. Figure 3.1 shows the configuragion of the experimental facility. The coordinate system shown in Figure 3.2 is used for the channel test section. The x-coordinate is in the direction of flow.

The settling chamber is equipped with a streamlined sheet metal shroud at the entrance which is covered with fiberglass gauze saturated with a light oil to keep dust from entering the channel. Immediately following the shroud is a honeycomb section made up of straws 1/4 inch in diameter and 8 1/4 inches long. The straws completely fill the cross-sectional area of the settling chamber. Adjoining the honeycomb section is a series of five screens with mesh

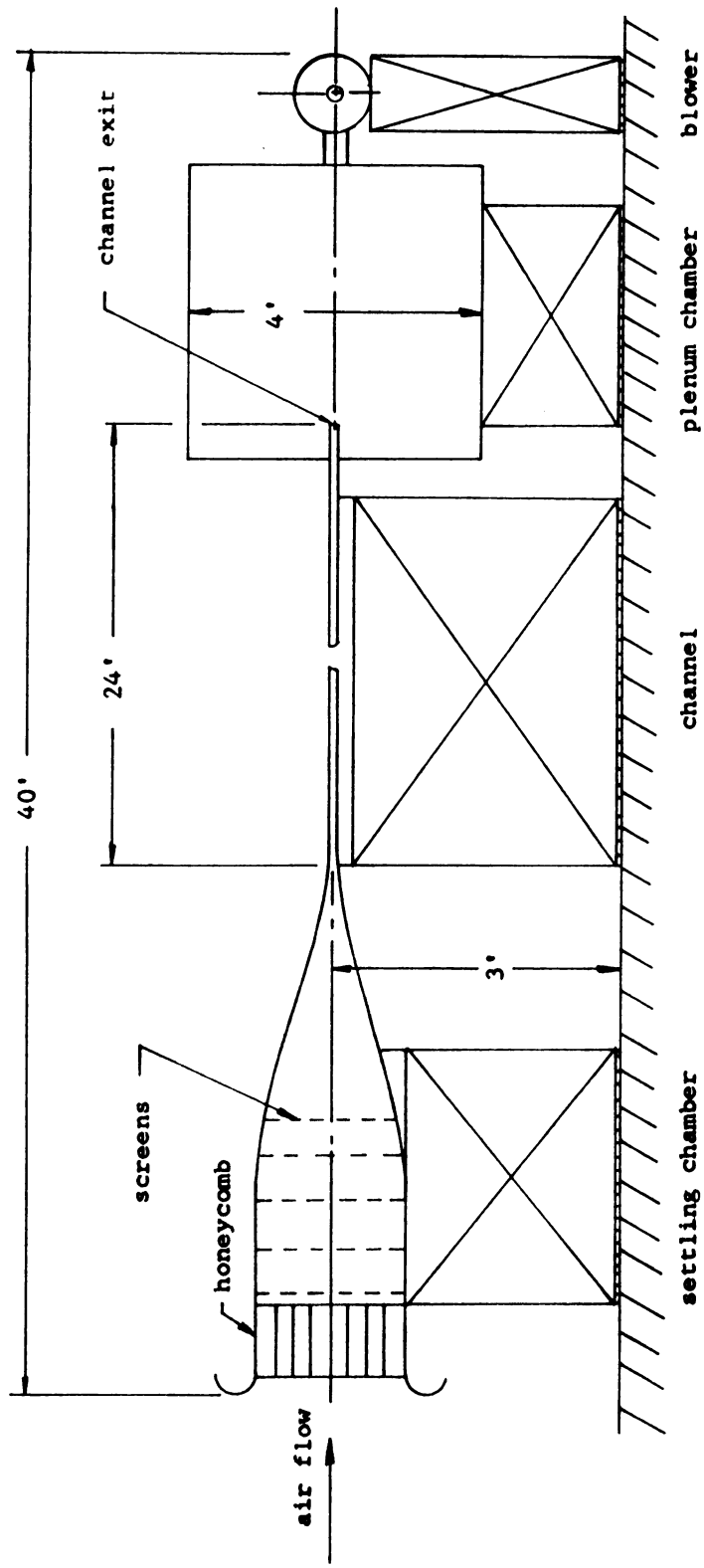

Figure 3.1 Experimental Facility

sizes of 40, 40, 80, 100, and 120, respectively. Further information concerning the screens is given in Table A-1 of Appendix A. The distance between of the screens is 7 inches. This part of the settling chamber is constructed in sections for easy variation of the screen configuration. Following the 120 mesh screen is the contraction. At the entrance of the contraction the cross-section is 12 inches high by 36 inches wide and at the exit the cross-section is 1/2 inch by 35 inches, with a total length of 6 feet. The contraction is constructed of sheet metal and wood. Heavy foam rubber is attached to the outside of the sheet metal and serves to dampen out unwanted vibrations. The shape of the contraction is a rather simple beam deflection curve, shown in Figure A-2 of Appendix A.

In this converging section the boundary layers are growing, so that at the beginning of the test section the flow is not uniform. The flow in the contraction is a developing flow as described in Chapter 4.

The test section is fabricated of rolled aluminum plates, machined aluminum strips and acrylic plastic sheets and strips. The bottom wall consists of 3 sections of 3/8 inch rolled, ground and polished aluminum plates. The joints are sealed and polished smooth. The top wall consists of 3 sections of 3/4 inch acrylic plastic sheets. The top sheets are joined together at the seams, which are sealed and polished smooth. The plastic top, now a single 24 foot section, can be lifted off to gain access to the interior of the

channel. The side walls are made of aluminum strips 1/2 inch by 1/2 inch, total length being 24 feet. These are machined and grooved on the top and bottom. The grooves are filled with bulk "O" ring stock which provides an excellent seal when clamped with large "C" clamps at increments of about one foot. Figure 3.3 shows a cross-section of the channel with "C" clamps not shown.

One of the most delicate parts of the experiment is keeping the plate gap constant. First, the bottom plate is leveled and flattened by the use of the adjusting nut beneath the aluminum plate. Next the channel is assembled, and with the use of a specially devised gapping instrument, the top plate is adjusted using the adjusting screws above the plastic. The gapping instrument is described in Figure A-3 of Appendix A. The downstream increment between the super-structure frames, as shown in Figure 3.3, is 2 feet. The total variation in gap, with the channel operating at 6,000 Reynolds number and with no flow, is +.001 and -.007 inches, respectively. This is a variation of 1.6% of the 1/2 inch gap at operating conditions.

The assembled test section thus is a 24 foot long rectangular duct with a constant 1/2 inch by 35 inch cross-section, all surfaces polished and with tightly sealed joints. Instrumentation is inserted into the test section, after assembly, through the exhaust plenum chamber.

The end of the channel enters into a 5 foot wide, 4 foot high and 8 foot long plywood exhaust plenum chamber. Attached to this

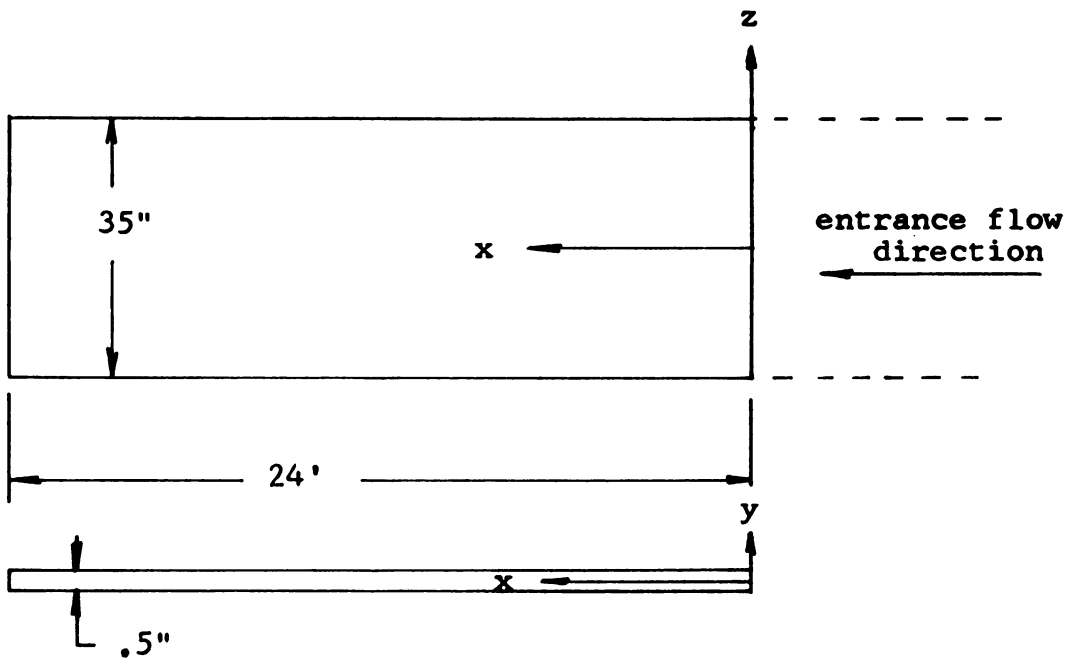

Figure 3.2 Coordinate System For Channel

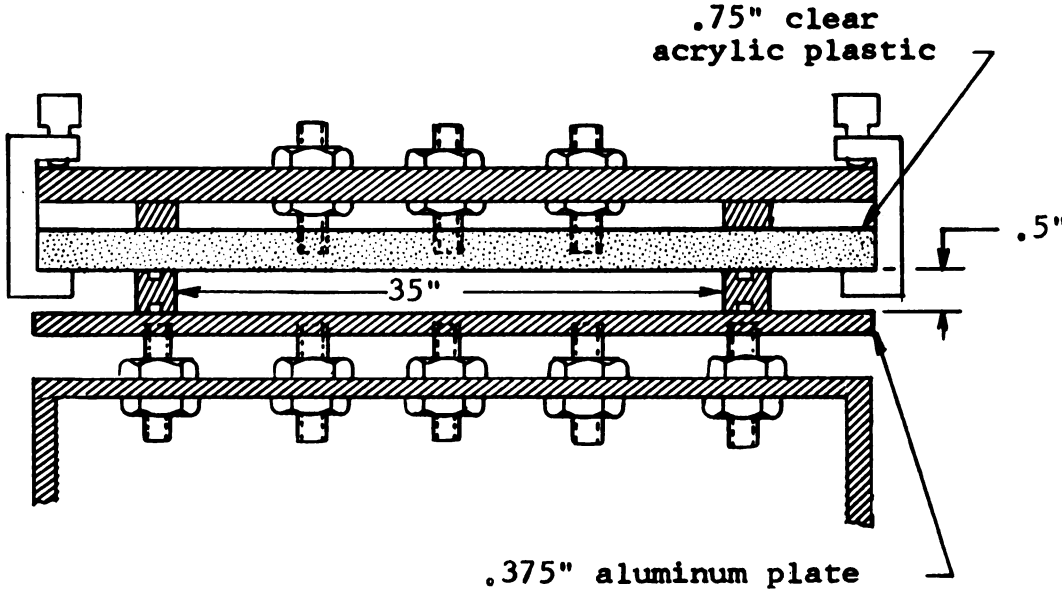

Figure 3.3 Channel Cross-section

exhaust chamber is an Aerovent Centrifugal blower, which is driven by a variable speed direct current motor. To eliminate vibrations both the blower and the channel are connected to the exhaust plenum by means of a light foam rubber which is backed with a cellulose plastic sheet. It is not necessary to seal this exhaust chamber as tightly as the entrance or the test sections.

During the course of the investigation a constant speed blower with a throttling valve also was tried. In addition, a diffuser on the channel exit, inside the exhaust plenum also was used at times. Neither of these changes made a measurable difference in the data.

3.2 Instrumentation--Innovated Equipment

The desire to keep the channel as smooth and as tightly sealed as possible, led to the conclusion not to drill a large number of access holes nor to disrupt joints for the mounting of instrumentation, hence, the instrumentation was introduced through the exhaust plenum. A special hot-wire probe was designed and built which was capable of traversing the flow in the y-direction, while in any x or z position. The probe, shown in Figure 3.4, was positioned in any x or z position with the use of a powerful electromagnet. The probe was placed in the interior of the channel test section, while the electromagnet, mounted on casters, was outside the channel on top of the plexiglas. When one moved the electromagnet the magnetic field acted through the plexiglas plate, interacted with the sheet

metal tail of the probe and provided controlled movement of the probe in the x and z directions.

The y-direction traverse was also accomplished with a magnetic field. A permanent horseshoe magnet, rotated by a servo motor outside the channel on top of the plexiglas, controlled the steel windmill of the probe. This windmill was directly connected to a threaded rod which thus drove the probe in the plus and minus y-direction. The traverse was calibrated outside the channel using a cathetometer. The accuracy of locating the probe in the y-direction was determined to be within .001 inches.

The stainless steel tubing supporting the hot-wire, when close to either wall had an angle of attack and this caused some drag force. To make sure that the tubing was not vibrating, the probe was placed in the exit of a uniform jet and traversed in the y-direction. The output of the anemometer showed no vibration due to this small angle.

3.3 Instrumentation--Commercially Available Equipment

In describing the instrumentation used, it is significant to know how it was used in the total system. The following list will describe the system and the instrumentation.

(a) Two Disa 55D05 constant temperature hot-wire anemometers in conjunction with a Disa 55D15 and a 55D10 linearizer were used. Outputs of both the linearizer and the anemometers

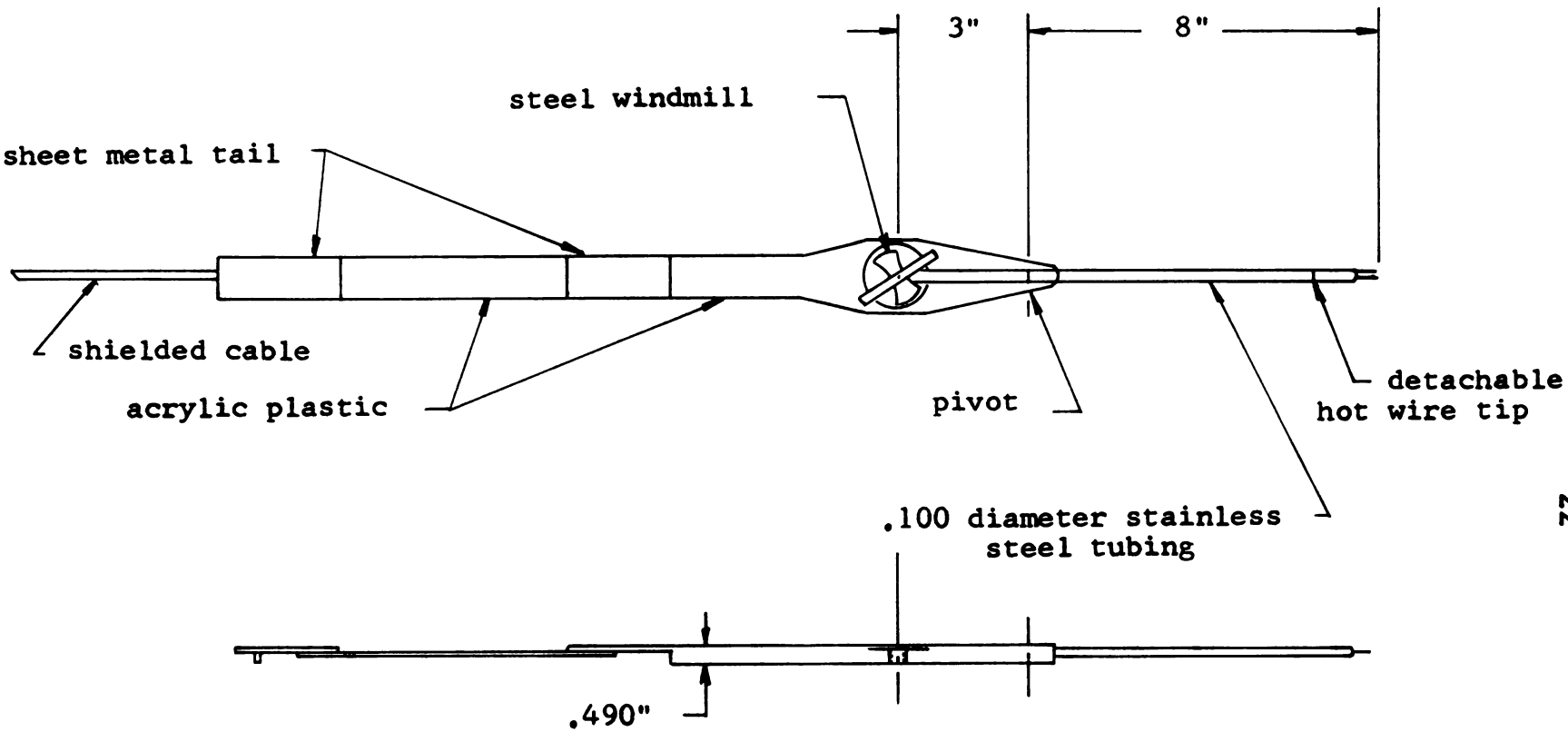

Figure 3.4 Hot Wire Probe

were recorded. Calibration of the hot-wire was done in a separate wind tunnel.

(b) Intensity readings were taken with a Disa 55D35 True R.M.S. Voltmeter using the output of the linearizer.

(c) High frequency noise of the anemometer was eliminated with the use of Thermo-System Model 1057 filters. Only the low pass filters were used.

(d) Both a Disa and a Digitec digital voltmeter were used in conjunction with the linearizers. The data for the velocity profiles taken from the digital voltmeters, was compiled and plotted using an 1800 I.B.M. computer.

(e) Spectral analysis of the anemometers and the linearizer signal was done with the use of a Quan Tech 304 wave analyzer.

(f) For visual records a Tektronix 564B fast writing scope was used in conjunction with a Tektronix C-40 camera. Polaroid film with an A.S.A. speed of 3,000 was used in the camera.

(g) Pressure measurements were taken with a Decker Delta Model 308 Differential Pressure instrument, using a one inch and a three inch (inches of water) transducer.

(h) In the sound system three different loud speakers were used to cover a range of frequency from 50 to 500 hertz. The loud speakers were: (1) J. B. Lansing 12 inch--Model D-216, (2) Jensen 12 inch--Model LMI-125, and (3) Altec 15 inch--803B. All three speakers were driven by the same power amplifier. The calibration of the wave amplitude will be discussed in Chapter 4.

CHAPTER IV

RESULTS AND DISCUSSION

4.1 Introduction

The results of linear stability theory show that transition to turbulence in channels should occur at Reynolds numbers much larger than those of previous investigations. This means that a laminar flow must be developed and maintained at a high Reynolds number. The development of the laminar flow is the main consideration in the construction of the channel. As the fluid exits from the last screen it enters a gradual contraction, where the boundary layers are growing under the influence of a favorable pressure gradient. Thus as the air exits from the contraction and enters the channel test section the velocity profiles are developing. This means that there is not a uniform velocity profile at the test section entrance. Figures 4.1, 4.2 and 4.3 show the developing velocity profiles at three different Reynolds numbers (based on average velocity and channel height). Examining Figure 4.1, at a Reynolds number of 2,210, there are three velocity profiles taken at x equal to one, two and three feet, with z equal to zero for all three profiles. Each velocity profile is normalized on the maximum velocity and then

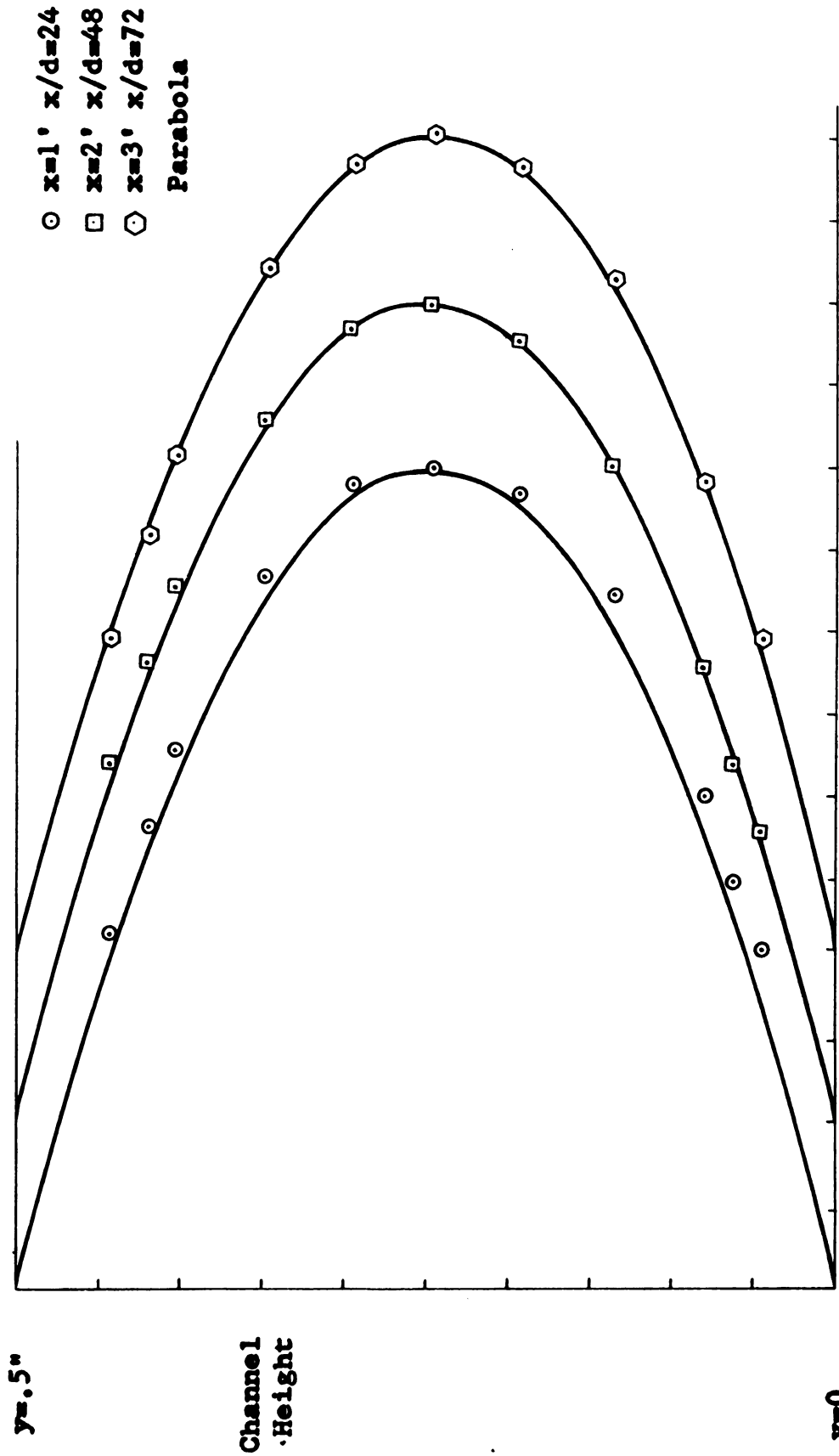

Figure 4.1 Developing Flow, Reynolds Number 2,210, z=0

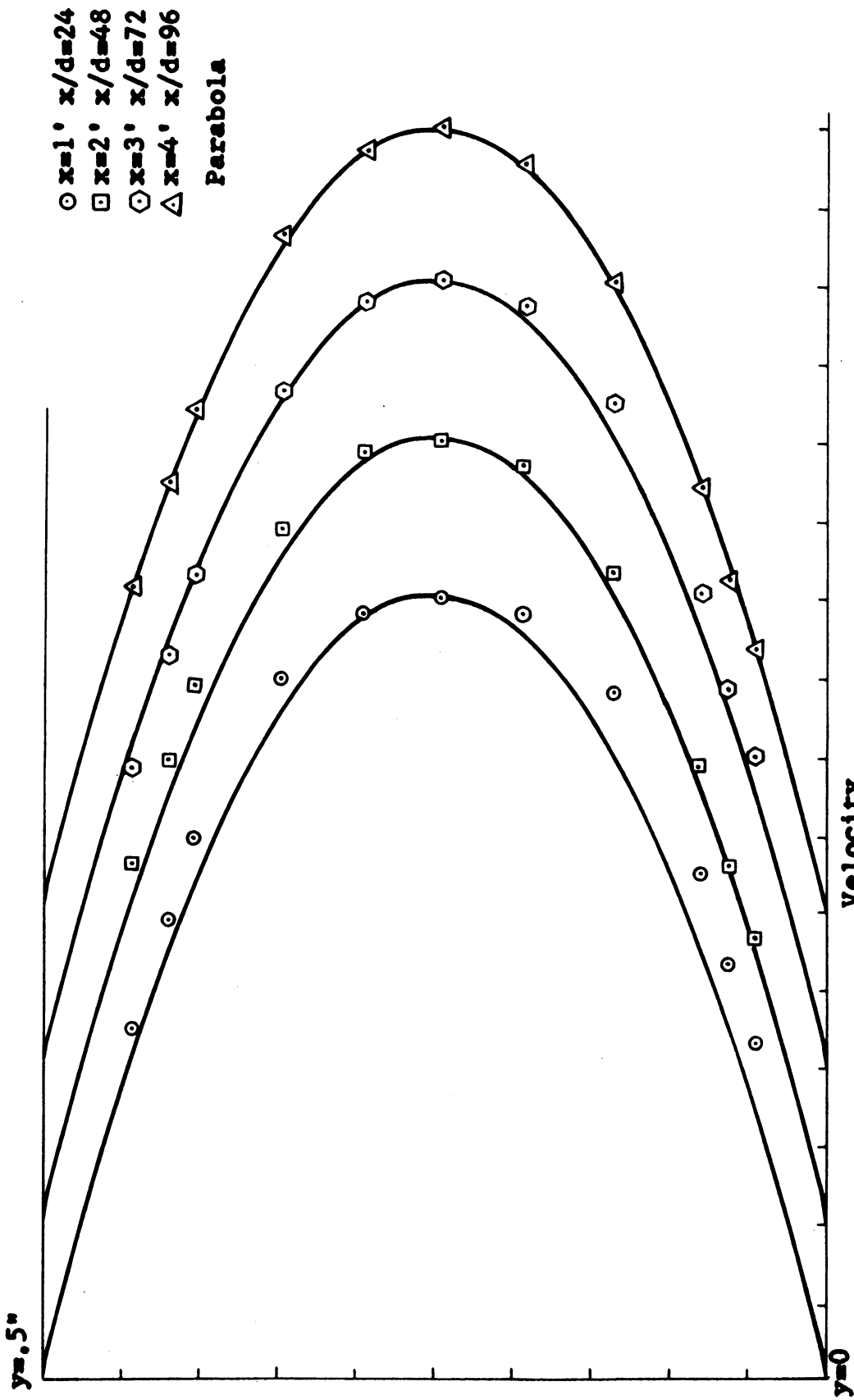

Figure 4.2 Developing Flow, Reynolds Number 3,710, z=0

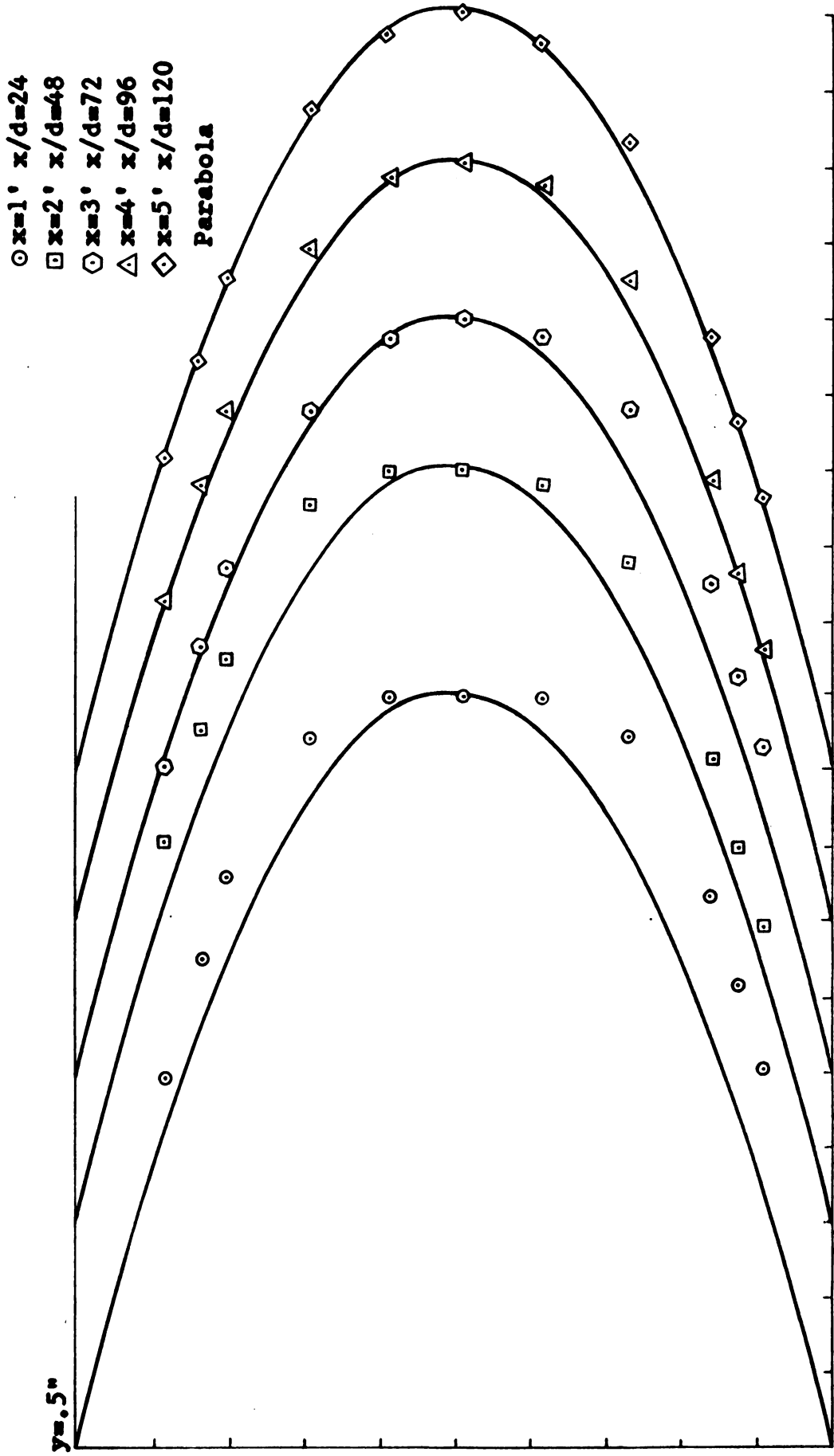

Figure 4.3 Developing Flow, Reynolds Number 6,160, z=0

compared with a parabola. For a Reynolds number of 2, 210, at approximately three feet, there is a parabolic profile and this profile remains parabolic throughout the final twenty-one feet of the test section. In Figure 4. 2, where the Reynolds number is 3, 710, the flow becomes and remains parabolic at x equal to approximately four feet and beyond. In Figure 4. 3, which is similar to Figures 4. 1 and 4. 2, the Reynolds number is 6, 160 and the flow becomes parabolic at approximately x = 5 feet. It is apparent that with increasing Reynolds numbers there is an increase in the entrance development length. Due to a developing flow at the entrance, it is difficult to compare the developing process in this channel with analytical studies, such as that done by H. Schlichting (1934).

Having attained a parabolic laminar flow at a Reynolds number of 6, 160 at x = 5 feet and z = 0, the next step is to examine the y-velocity profiles off the z-coordinate ($z \neq 0$). Figure 4. 4 contains four velocity profiles, all taken at a Reynolds number of 5, 920 and at x = 5 feet, and at z = 0, 9, 13 1/2, and 15 1/2 inches, respectively. The total width of the channel is 35 inches; this places the profile, at z = 15 1/2 inches, two inches from the channel side walls. All four profiles in Figure 4. 4 are parabolic. From the profile aspect the channel is two-dimensional over approximately thirty-one inches of the thirty-five inch wide channel.

Additional profiles are taken with a 3/16 inch diameter wire placed at the entrance of the channel test section. The wire trips the

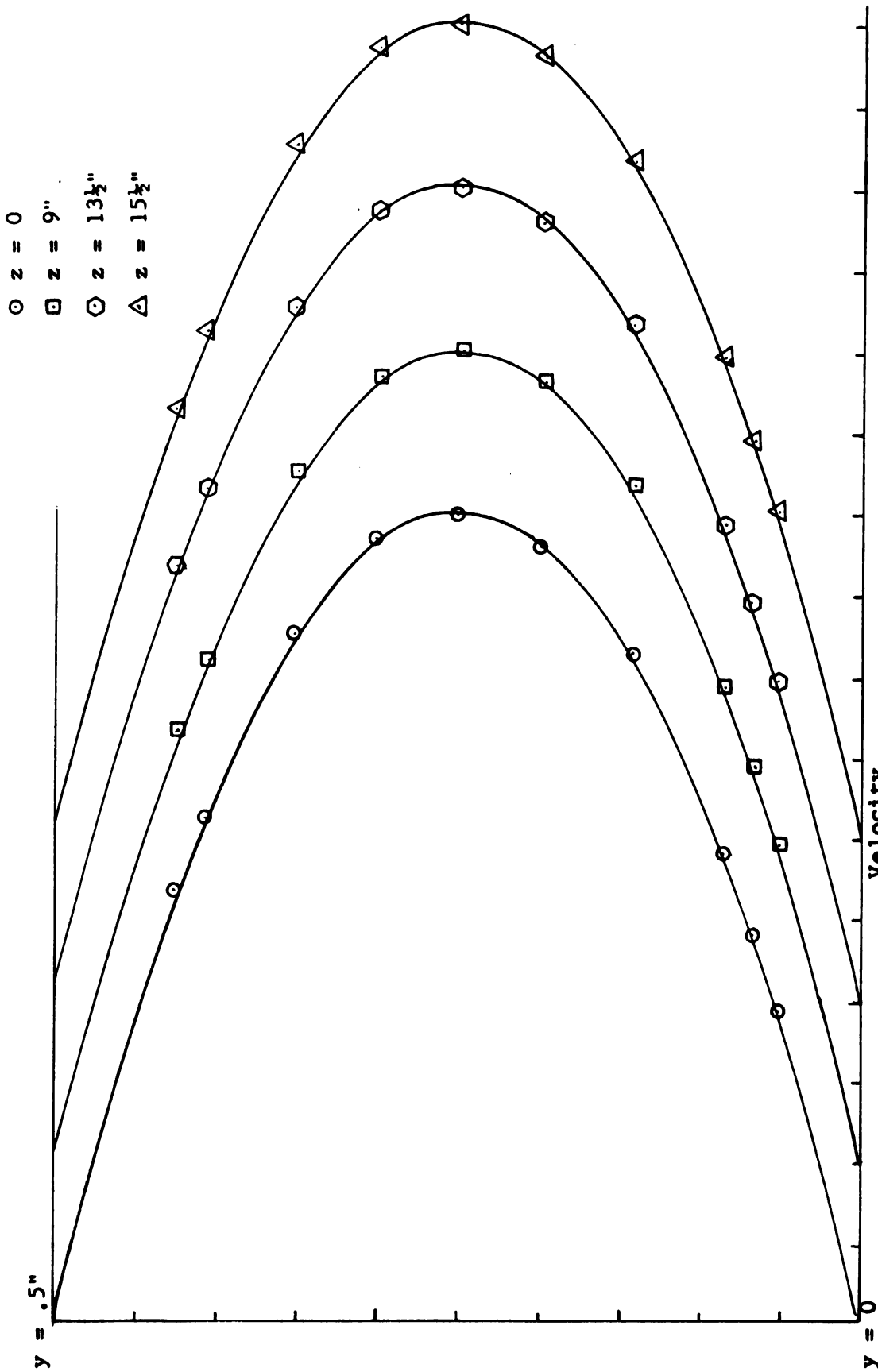

Figure 4.4 Velocity Profiles at Varying z-positions, x = 5'

flow and induces turbulence. Below a Reynolds number of 1, 700 the flow is laminar; for a minimum critical Reynolds number this is high compared to a minimum of approximately 1, 000 by Narayanan and Narayana and many others. However, the 1, 700 is not a true minimum since only a 36% blockage of the flow is caused by the trip wire.

The profiles taken with the trip wire in the channel are shown in Figure 4. 5. The y-coordinate traverses are taken at x = 5 feet and z = 0, at Reynolds numbers of 2, 750 and 6, 350. Both are normalized on the maximum velocity and compared to a parabola and a 1/7 power law curve. At a Reynolds number of 6, 350 the data compares very favorably with the 1/7 power law and has a turbulent intensity of 5%. This is high compared to Laufer's (1951) 3. 5% intensity reading for a Reynolds number of 12, 300, but, as Laufer demonstrated, the percent intensity increases as the Reynolds number is decreased.

With the trip wire removed from the channel a 1/8 inch diameter pin was injected through the side wall at x = y = 0 and z = - 17 1/2 inches, to determine the effect of an induced corner disturbance. In this configuration, the pin extends 1/4 inch into the flow at the side wall. Figure 4. 6 shows the results with and without the pin, at a Reynolds number of 5, 900 and an x-position of five feet. The top two traces are taken with the hot-wire placed at the z = 0 coordinate, the first trace taken without the pin and the second with the pin; both are

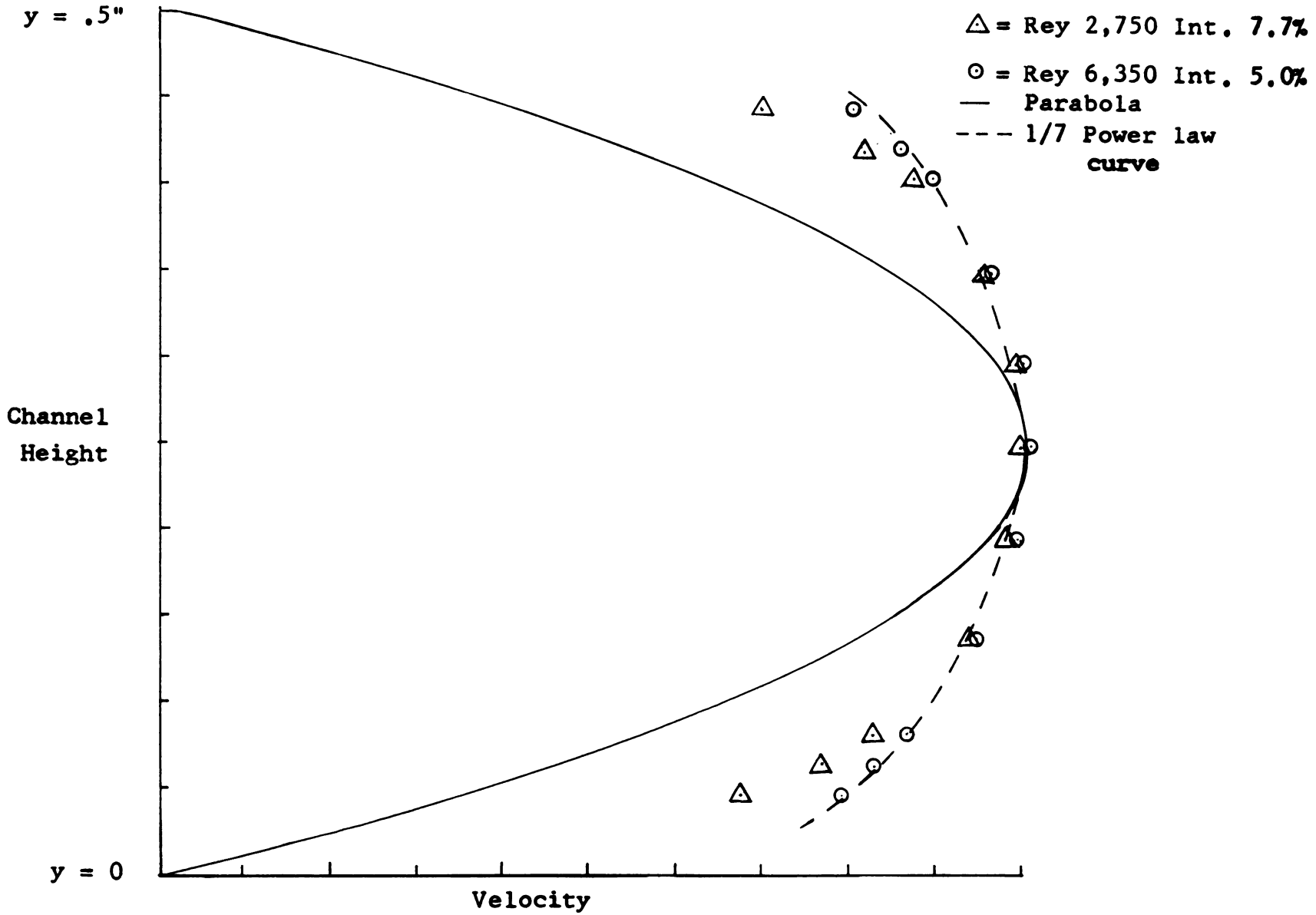

.187" Diameter Rod at Entrance - x = 5', z = 0, x/d = 120

Figure 4.5 Velocity Profile with Trip Wire

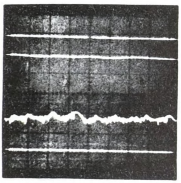

No Pin
z=0
Pin

Pin
z=-14"
No Pin

50 millisec./div.

Figure 4.6 Pin Injected Into Flow
x=5', y=0, x/d=120
Rey=5,900
Third trace vertical scale one-hundred times larger than the other three traces.

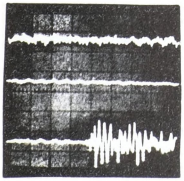

Channel operating at Rey=6,500

Channel not operating

Lightly touching the channel

50 millisec./div.

Figure 4.7 Vibrations of the Test Section
Output Accelerometer Attached to exterior of the channel at x=8', z=0, x/d=192

smooth laminar flows. The third and fourth traces are with the hot-wire probe placed at z = - 14 inches. The third trace is with the pin injected and shows turbulent fluctuations. From the second and third traces, both with the pin inserted, there is a change from laminar flow to flow with turbulent fluctuations. This indicates that the pin causes a region of turbulent fluctuations near the side wall to coexist with a laminar flow towards the channel center. Hence, if a large disturbance exists in the corners in the entrance it is a definite generator of turbulence. Great care was taken to eliminate all such protrusions and the resulting corners produced no adverse effects.

A check was also made for vibrations on the channel test section caused either by the blower or other external factors such as building vibrations. These vibrations could possible induce higher intensity disturbances in the fluid flow. The blower and the exhaust plenum were isolated from the test section, as described in Chapter 3. An accelerometer was placed on the exterior surface of the plexiglas sheet at approximately the x = 8 foot position. Figure 4.7 shows the output of the acceletometer; the top trace is with the flow system operating at a Reynolds number of 6,500, the middle trace is with the flow system totally inoperative. The bottom trace shows the size of a disturbance, while the channel is inoperative, which is caused by a light touch of a finger on the exterior surface of the plexiglas sheet, sixteen feet downstream of the accelerometer.

From the top and middle traces, it is perceived that physical vibrations of the flow system cause a detectable increase in vibrations of the plastic wall of the channel. However, the amplitude of the vibrations is only slightly increased between the inoperative state and the operative state of the flow system. Therefore, it seems plausible that the intensity of velocity fluctuations in the flow is due mainly to entrance region effects and pressure fluctuations caused by the fan which are traveling upstream and not by the physical vibrations. It is noted that loud noises and sharp physical vibrations induce transition as confirmed by experiments with this channel.

4.2 The Natural Transition Process

The transition Reynolds number, referred to in the following paragraphs, is the Reynolds number at which the first slug is detected. This Reynolds number is easily detected due to an abrupt discontinuity in the velocity signal between the laminar flow and the turbulent slug. This is shown in Figure 4.10; the turbulent slug differs from the laminar flow by amplitude and frequency variations of the velocity fluctuation of about two orders of magnitude.

One of the main parameters that governs transition is the intensity of the velocity fluctuation in the flow. It is a general rule that if the intensity can be lowered, the transition Reynolds number will be increased. There are possible exceptions to this; a case being where two flows have the same intensity but are made up of different frequency bands. The transition Reynolds number will

most likely be different for the two situations if the bands are narrow; however, if the bands are wide then the transition Reynolds numbers will most likely be identical.

Secondly, vorticity may also be responsible for causing transition. Vortex stretching in the corners could cause turbulent fluctuations in the corners near the side wall; the turbulent fluctuations could coexist with laminar flow in the center of the channel, the results being similar to that of having a pin injected into the side wall. For this experiment this situation does not occur in the natural transition process.

Taylor-Görtler vortices are also a possible mechanism for initiating transition. These vortices are caused by the turning radius in the converging entrance chamber. This was initially one of the main considerations for the construction of a very gradual contraction.

As stated earlier in Chapter 4, the velocity fluctuation intensity is believed to be made up primarily of two components; the entrance region effects and pressure fluctuations caused by the blower. Only by the use of a sonic throat can the pressure fluctuations of the blower be eliminated. A sonic throat is not employed in this experiment and there is apparently no way of measuring the effect of each of these separately. From the author's own experience, the entrance region effect seems to dominate the fluctuation intensity.

For this channel facility, a Reynolds number of 6, 700 (based on average velocity and channel height) is the largest attained for a parabolic laminar flow. This is 87 percent of that predicted by linear theory. The velocity fluctuation intensity of the parabolic laminar flow at the above Reynolds number is .3 percent. The intensity is made up mainly of fluctuations in a frequency band of 0 to 10 hertz.

When the Reynolds number is increased to a value slightly greater than 6, 700 the natural transition process begins to occur, but only in the section of the channel where there is a parabolic flow. The parabolic flow is developed at approximately $x = 5$ feet and upstream of this point in the test section the flow is stable. Even when the Reynolds is increased to a maximum of 10, 000, the flow in the five foot entrance region is stable.

Using the theory of small disturbances, T. E. Chen and E. M. Sparrow found the critical Reynolds number decreasing monotonically with increasing distance from the channel entrance, approaching the value of 7, 700 in the developed parabolic profile. This result implies that the developing flow is more stable than the parabolic flow.

One unusual fact about the channel is that the stable entrance region length of five feet remains a relative constant when the Reynolds number is varied between 6, 700 and 10, 000. This indicates that although the developing length increases beyond the five foot

length with increasing Reynolds numbers, the transition Reynolds numbers of the profiles beyond five feet are less than a Reynolds number of 10, 000.

Variation of the fluctuation intensity is accomplished by entering grids of different diameters and different mesh sizes in the settling chamber beyond the last screen. More details about the grids are in Table A-2 of Appendix A. Figure 4. 8 is a plot of intensity versus transition Reynolds number. The intensity in this plot is measured at the (x = y = z = 0) entrance of the test section. The plot demonstrates that as the intensity is decreased the Reynolds number increases monotonically. An intensity of 5 percent causes transition to occur at a Reynolds number of 2, 000. The grids produce fluctuations which at x = 0 have most of their energy in a low frequency band of 0 to 30 hertz.

The natural transition process itself can best be explained by looking at the output signal from the hot-wire anemometer at the x = 6 foot position in Figure 4. 9. Looking from top to bottom, the traces are in the order of increasing Reynolds numbers. The top trace is at a Reynolds number of 6, 300 and from the trace it is observed that there is a laminar flow. The velocity profile is considered parabolic at this location and Reynolds number. When the Reynolds number reaches 6, 700 a large disturbance is detected; this is the beginning of the development of the turbulent slug. It is observed that the flow oscillates between a laminar and turbulent flow. The

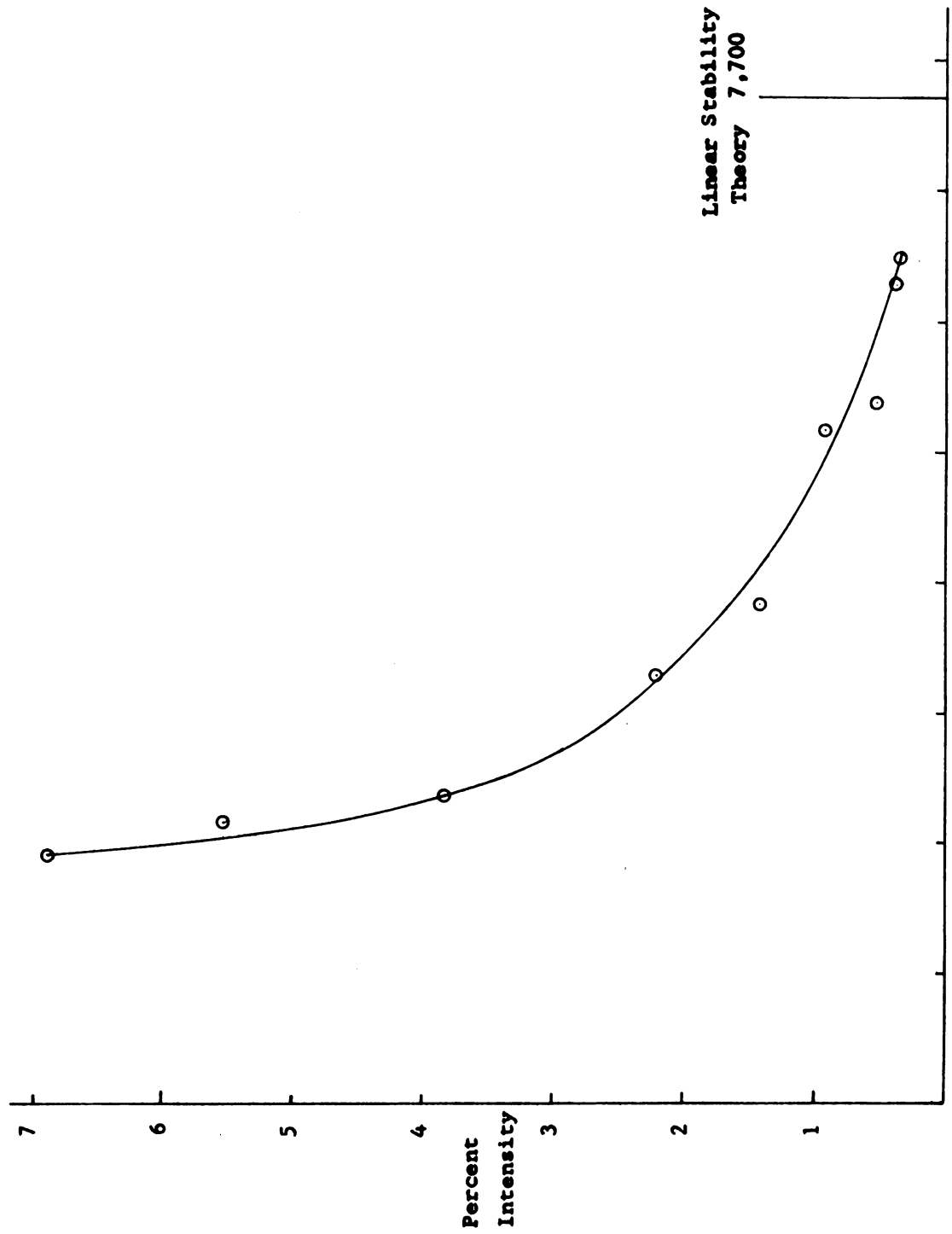

Figure 4.8 Intensity Variations Using Grids

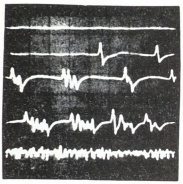

Rey=6,300
Rey=6,700
Rey=6,900
Rey=7,000
Rey=8,500

.5 sec./div.

Figure 4.9 Bursting Process With Increasing Rey. No.
Hot Wire Output Anem.
x=6', y=0, z=0, x/d=144
V. Scale 20 millivolts/div.
Blocking Capacitor Employed

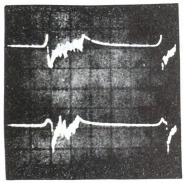

z=4"

z=-3"

.2 sec./div.

Figure 4.10 Two-Dimensional Slug
Hot Wire Output Anem.
x=9'4", y=0, x/d=224
Rey=6,900
V. Scale 100 millivolts/div.
Blocking Capacitor Employed

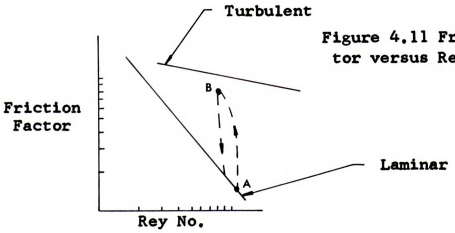

Figure 4.11 Friction Factor versus Rey No. Plot

initial spike of each disturbance appears at regular intervals. Figure 4.9 does not fully describe the shape of the disturbance due to the fact that a blockage capacitor is employed.

Before examining the disturbances at the higher Reynolds numbers as in Figure 4.9, the disturbances at a further downstream position are examined. In Figure 4.10 two hot-wire probes are positioned at the x = 9'4" station, one wire located at z = -3 inches and the other wire at z = 4 inches. From the traces it is obvious that the slug of turbulence has grown in size and the frequency of the fluctuations inside the slug is considerably higher than at the upstream position. The simultaneous traces of both hot-wires indicate that the slug exists across the width of the channel. It is concluded that the slug of turbulence is initiated at approximately the position where the flow becomes parabolic, as shown in Section 4.5, and is two-dimensional at this position and is growing in size as it moves downstream. Sherlin determined that the leading edge of the slug travels at a speed of 1.77 times the average velocity while the trailing edge of the slug decreases in speed as the Reynolds number is increased. Wygnanski and Champagne (1970) demonstrated, for a pipe flow, that fluid was being entrained at both the leading and trailing edges of the burst. It is assumed that the same entrainment of the slug occurs in a channel.

Returning to the increasing Reynolds numbers shown in Figure 4.9, the effect of going from a Reynolds number of 6,900 to 7,000

causes the bursts to fill in the laminar flow region between the initial spike of each slug. The bottom trace is at a Reynolds number of 8, 500 and shows a fully turbulent flow. The turbulent bursts contain much larger disturbances than the fully turbulent flow. The time interval between the initial spikes varies randomly with time between 1. 1 and 1. 5 seconds. The explanation of what causes the regularity of repetition of bursts is the fact that there is an increase in the shear stress at the walls in the turbulent slug; this increases the friction factor and thus causes a decrease in the mean velocity. When the slug exits from the channel the mean velocity increases and causes another burst. Prandtl (1934) explained this phenomenon similarly. Figure 4. 11 is a plot of friction factor versus Reynolds number, there are two curves on the plot; one laminar and the other turbulent. If the flow is laminar and the Reynolds number is increased to point A, where a burst is initiated, the slug grows and travels down the channel increasing the friction factor of the entire channel and decreasing the mean velocity. At point B the slug exits from the channel, the friction factor decreases and the mean velocity increases and the flow again reaches point A and the whole cycle reoccurs. Sherlin and Breslin used dye and a puffer device to disturb the laminar flow and generate the slug of turbulence, therefore, they did not note the regularity between bursts.

If there is a variation in the mean velocity it should easily be detected in the more stable developing flow at the entrance of the test

section. Figure 4.12 is the linearized output of the hot-wire signal at the entrance of the test section. The top trace is for a Reynolds number of 5,000, for this trace there are no turbulent slugs in the channel. The second trace is at a Reynolds number of 6,900 and characterized by large low frequency oscillations. Beyond the five foot entrance length, at this Reynolds number, the flow is oscillating between a laminar and turbulent slug flow. The oscillation at the entrance is a variation of 2 percent of the velocity of the flow. The bottom trace is at a Reynolds number of 8,500 and the entrance flow shows no variation in the flow rate, due to the fact that beyond the entrance length the flow is fully turbulent.

It is assumed that the first stages of the development of the turbulent slug are associated with linear stability theory. As the slug is formed and fills the channel the flow rate drops due to the increased shear on the walls and appears to stabilize the flow such that initiation of the burst is stopped. The burst is then washed from the channel accompanied by an increased flow leading to another instability. This process continues for a range of Reynolds numbers slightly greater than the transition Reynolds number and results in a surprisingly regular oscillatory phenomenon.

4.3 The Initial Stage of Transition

The next step in the present study is to examine the flow field before the first slug of turbulence is detected. Figure 4.13 shows

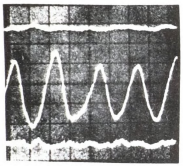

Rey=5,000

Rey=6,900

Rey=8,500

.5 sec./div.

Figure 4.12 Entrance Region
Hot Wire Output Linearizer
x=1', y=0, x/d=24
V. Scale 20 millivolts/div.

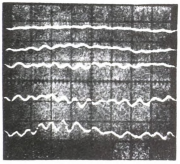

y=.218"

y=.200"

y=.160"

y=.110"

y=0

50 millisec./div.

Figure 4.13 Laminar Flow-Fast Sweep, Rey=6,250
Hot Wire Output Anem.
x=8', z=0, x/d=192
V. Scale 2 millivolts/div.

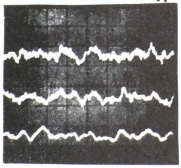

y=.200"

y=.160"

y= 0

.5 sec./div.

Figure 4.14 Laminar Flow-Slow Sweep, Rey=6,250
Hot Wire Output Anem.
x=8', z=0, x/d=192
V. Scale 2 millivolts/div.

y=.200"

50 millisec./div.

Figure 4.15 Laminar Flow
Rey=6,600
Hot Wire Output Anem.
x=8', z=0, x/d=192
V. Scale 2 millivolts/div.

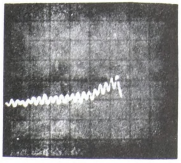

50 millisec./div.

Figure 4.16 First Burst
Hot Wire Output Anem.
x=9'8", z=0, y=.200" x/d=232
Rey=6,700
V. Scale 2 millivolts/div.

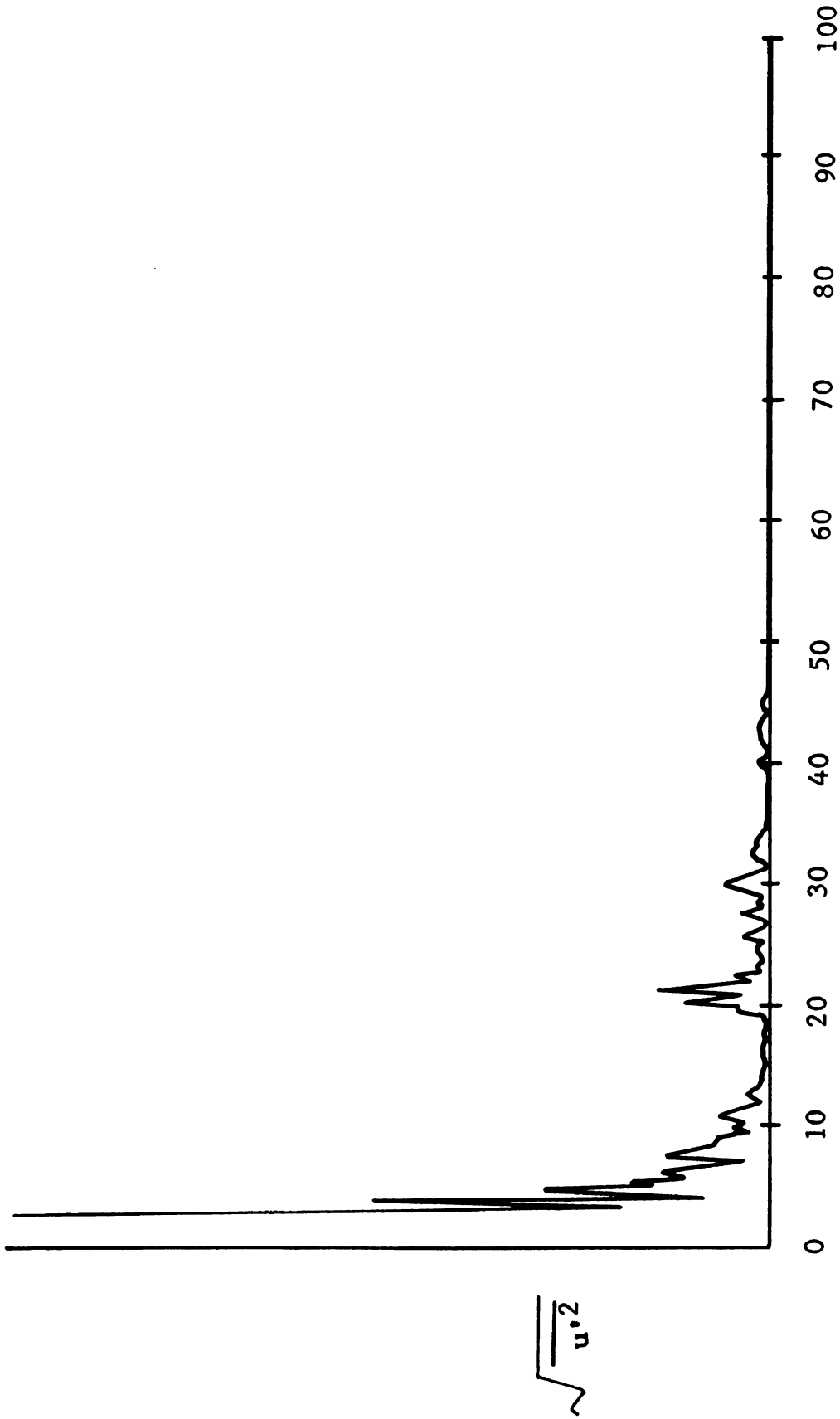

Figure 4.17 Frequency Spectrum Rey=6,600, y=0

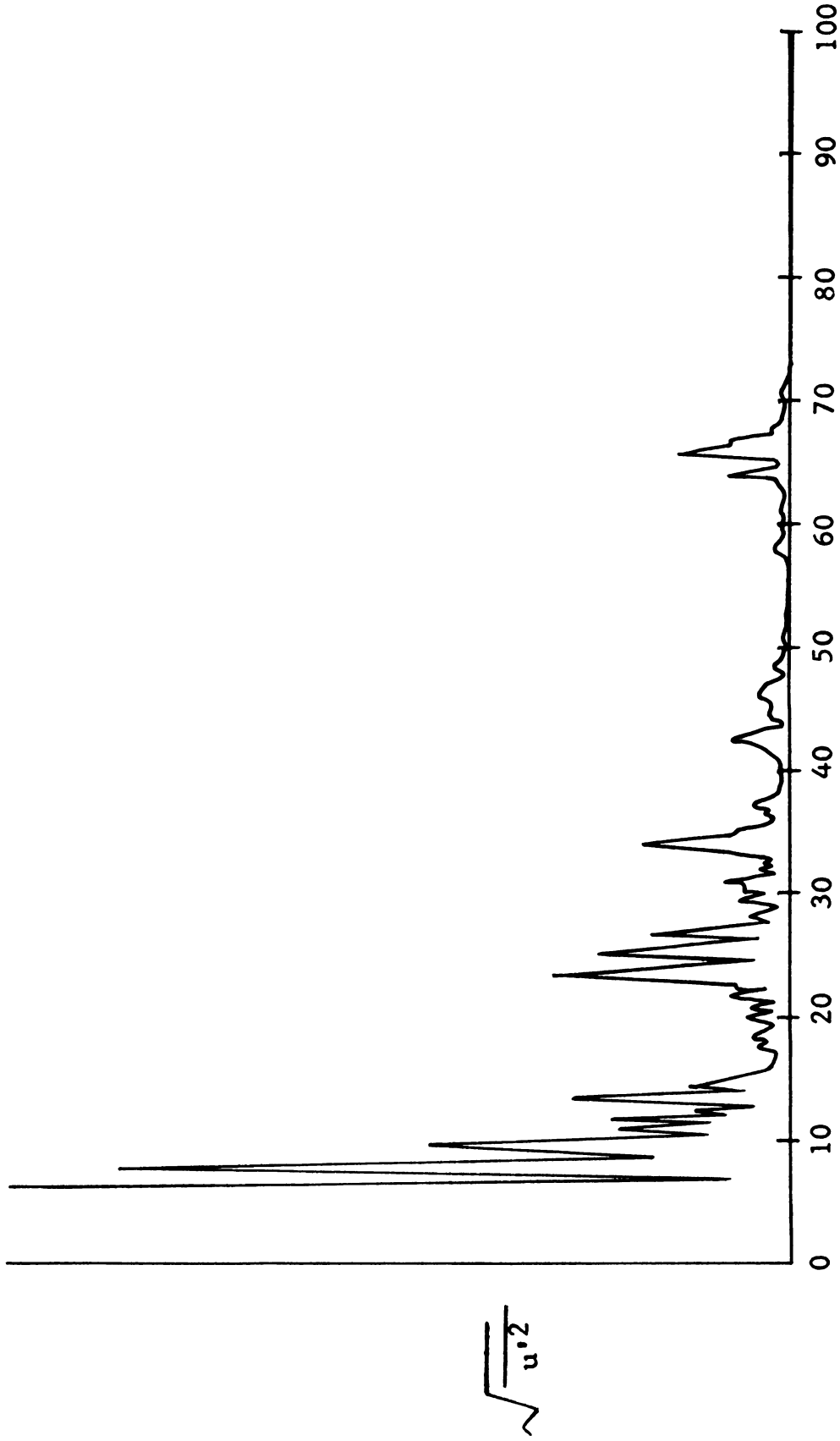

Figure 4.18 Frequency Spectrum Rey=6,600, y=.204"

the hot-wire output of five signals, at a Reynolds number of 6, 250. A Reynolds number of 6, 250 is 450 below the point at which a turbulent slug is detected. The bottom trace is taken at y = 0, the location of the maximum velocity in the channel, and each additional trace is taken at a position closer to the top wall, respectively. Near the wall there is a wave of approximately 30 hertz; the same wave is observed at the other wall. It is noted for reference that the vertical gain in these pictures is much larger than that of previous figures showing the turbulent bursts. Also, the intensity of the flow at the center line is .3 percent. Figure 4.14 has three traces of varying y-positions, but at a slower sweep rate than Figure 4.13. The figure which shows that at all y-positions the fluctuations have frequencies of 0 to 20 hertz.

If the Reynolds number is increased to 6, 600, with the hot-wire at the point of maximum velocity (y = 0), there is no noticeable change in signal from the previous Reynolds number of 6, 250. However, at a distance of $y > h/4$ the flow disturbance oscillates between a somewhat irregular wave of 25 to 35 hertz and a very regular wave of 50 to 70 hertz. The oscillation between these two frequencies is shown schematically:

Figure 4.15 shows a wave of about 67 hertz at a Reynolds number of 6, 600. A spectral analysis of the signals is shown in Figures 4.17

and 4.18, with y = 0 and -.204", respectively. The spectral analyzer slowly sweeps through the frequency range of 0 to 100 hertz. Since the period of oscillation of the signal between the two frequencies is of the order of 500 milliseconds, the analyzer averages the signal and shows frequencies in both bands, 35 and 67 hertz, as shown in Figure 4.18.

If the Reynolds number is increased to 6,700, on the verge of bursting, the hot-wire signal trace shows an almost perfect sine wave pattern of greater than 70 hertz. This trace is shown for the hot-wire at x = 9 feet 8 inches, z = 0 and y = .200 inches in Figure 4.16. The sine wave pattern occurs 300 milliseconds before the first burst is detected. The burst is not shown in Figure 4.16 as the higher frequencies and larger amplitudes in the burst are not observable for such a small vertical scale setting of the scope. Thus, the disappearance of the trace coincides with the initiation of the burst. The process is shown schematically:

[25 - 35 hertz] → [regular wave, 50 - 70 hertz] → [sine wave, >70 hertz] → Burst

Linear stability theory, described in Chapter 2, determined that at the minimum critical Reynolds number the frequency is 86.5 hertz for this channel, which is close to the experimental results described in the previous paragraph.

A significant growth in amplitude of the waves before the burst is not detectable, except during the last cycle of the laminar oscillation. This might be due to the fact that the hot-wire is not at

the exact position where the first burst appears, because the exact position cannot be located. The first burst occurs somewhere within the final twenty-one feet of the test section, this position probably varying in time.

With two hot-wires placed in various positions in the flow field no localized turbulent spots are observed, as have been detected in a flat plate boundary layer flow. The burst appears to be uniformly distributed across the width of the channel and does not vary with the z-coordinate.

4.4 Artificial Excitations of a Plane Poiseuille Flow

If a sound wave is introduced into the channel by placing a loud speaker at the entrance of the settling chamber, transition can be initiated at a lower Reynolds number. In this instance, the loud speaker is driven by a power amplifier at variable frequencies and the disturbances that are introduced by the loud speaker are much larger than other outside disturbances. A hot-wire probe is placed where the flow is parabolic, at $x = 6$ feet. At each individual frequency the flow rate of the channel is increased to the point where a turbulent burst appears, which is the transition Reynolds number. The amplitude of the sound waves at each frequency is calibrated by means of the hot-wire anemometer, setting the channel Reynolds number at 900 for each frequency and accepting only sine waves from the output of the anemometer. The amplitude of the waves, as determined from the output signal of the anemometer, is kept at a

constant level, by varying the power amplifier input signal to the loud speaker. Using this method of calibrating the amplitude of the waves with a hot-wire signal at low velocities, the problems of dealing with the resonant frequency of the channel and the loud speaker are reduced.

The results of the sound test, using the procedure described in the preceeding paragraph, are shown in Figure 4. 19, a plot of frequency versus transition Reynolds number. The frequency in this plot varies between 50 and 500 hertz, using three different speakers to attain this range. The curve has four minimum nodes, the minimum transition Reynolds number is 5, 280 at 370 hertz. The lowest frequency node is at a Reynolds number of 5, 660 at 130 hertz. Thus, the finite waves produced by the loud speaker generate a transition loop of more than one node, far to the left of the neutral linear stability loop. The transition process induced by the finite waves has the same intermittent bursting characteristic as shown previously.

There are two inherent characteristics of a sound wave that should be noted. First, the wave travels at the speed of sound and not at the propagation speed of the fluid. Second, while it is more desireable to have a wave induced at a specific location, where the flow is parabolic, in order to determine a growth rate, in this experiment the sound wave is injected into the entire flow field.

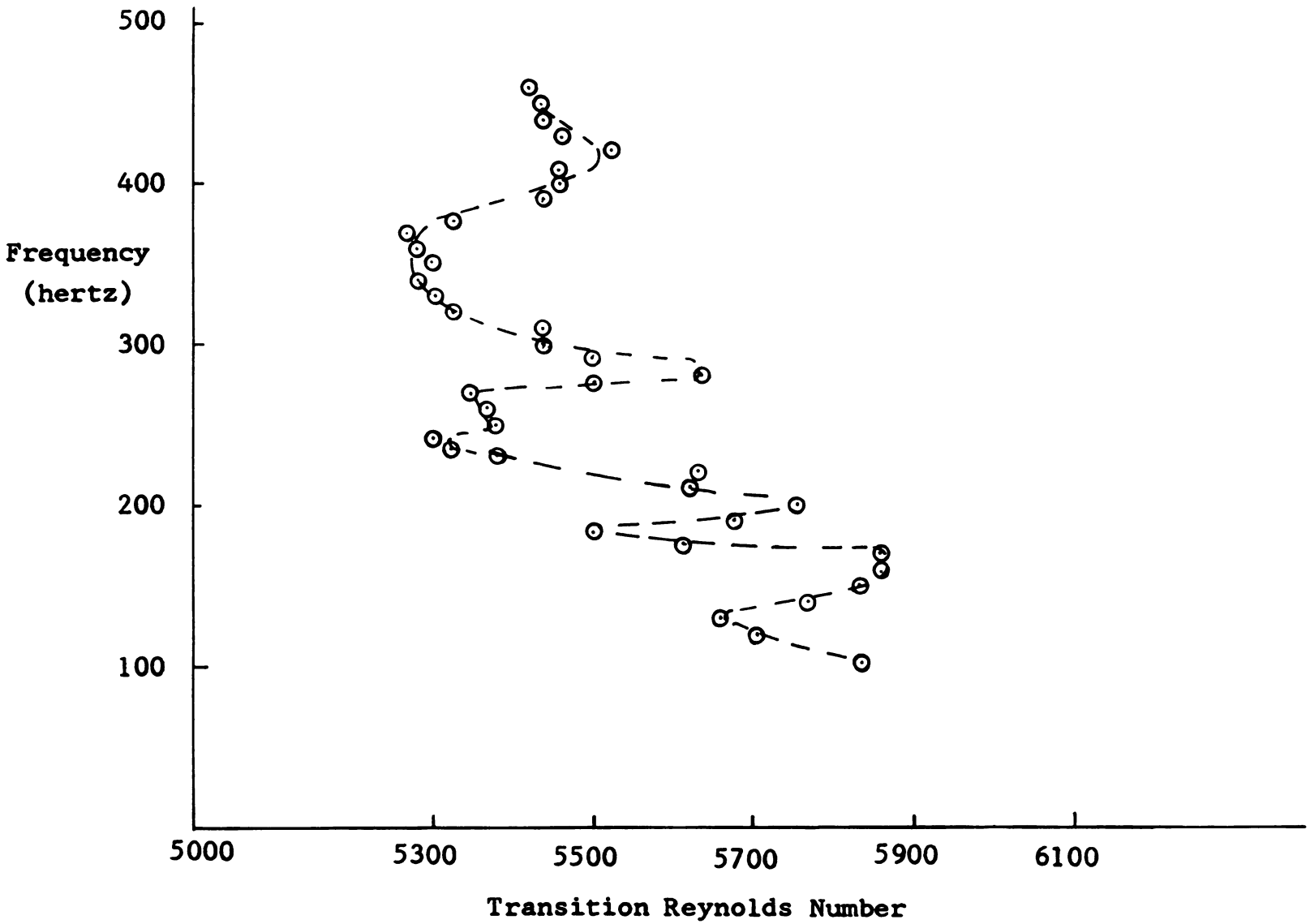

Figure 4.19 Finite Waves Induced by Sound

4.5 Details of the Turbulent Slug

A closer examination of the turbulent slug, at varying x-positions, along with the laminar flow occurring between slugs are the main concerns of this section. The slug at x = 10 feet and a Reynolds number of 6,900 is seen in Figure 4.20 in which the oscillating bursting process is taking place. Note that at the leading edge of each slug there is a large positive spike in the velocity vector. The spike is increasing in size as x increases. An electronic counter, used to measure the time intervals between the slugs, is triggered on this initial spike. This time interval varies between 1.1 and 1.5 seconds. Between the trailing edge of a slug and the initial spike of the following slug there is a laminar flow, and an increase in the velocity is observed, which agrees with the variation in the mean velocity described in the transition process of Section 4.2.

Before the bursting process occurs there is a parabolic laminar flow. When the Reynolds number is increased and the flow is intermittent between a turbulent slug and a laminar flow the velocity profile also varies between being a parabolic and a turbulent profile. Figures 4.21 through 4.23 are the hot-wire linearized signal at a Reynolds number of 6,900 and x = 10 feet. The differences between each figure is the y-position from the center line. In Figure 4.21, at the center line of the channel, the average velocity of the slug is smaller than the velocity of the laminar flow; whereas in

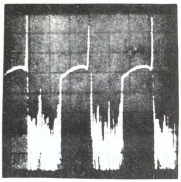

.5 sec./div.

Figure 4.20 Turbulent Slug
Hot Wire Output Anem.
x=10', y=0, z=0 x/d=240
Rey=7,000
V. Scale 20 millivolts/div.

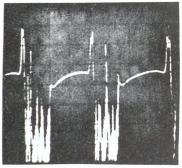

.5 sec./div.

Figure 4.21 Profile Shift, y=0
Hot Wire Output Linearizer
x=10', y=0, z=0 x/d=240
Rey=6,900
V. Scale 100 millivolts/div.

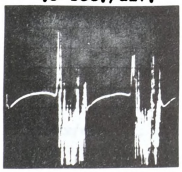

.5 sec./div.

Figure 4.22 Profile Shift, y=.097"
Hot Wire Output Linearizer
x=10', y=.097", z=0, x/d=240
Rey=6,900
V. Scale 100 millivolts/div.

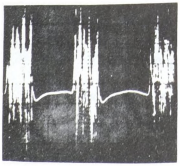

.5 sec./div.

Figure 4.23 Profile Shift, y=.206"
Hot Wire Output Linearizer
x=10', y=.206", z=0, x/d=240
Rey=6,900
V. Scale 100 millivolts/div.

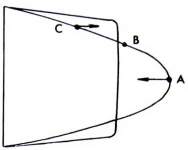

Figure 4.24 Profile Shift Between a Laminar Flow and a Turbulent Slug
Point A - Figure 4.21
Point B - Figure 4.22
Point C - Figure 4.23

Figure 4. 23 the average velocity of the slug is larger than the velocity of the laminar flow. A more descriptive diagram of this is shown in Figure 4. 24.

Figures 4. 25 and 4. 26 show large low frequency fluctuations in the corners while the main portion of the channel is a laminar flow. As described earlier, the burst occurs across the width of the channel at the same instant; there are no protruding angles from the corners separating turbulent and laminar flow. It is concluded that the fluctuations in the corners do not cause transition. Figures 4. 27 and 4. 28 show a decrease in frequency content of the slug in the corners of the channel.

Finally, it is noted that the slug develops from a low frequency oscillation into a mass of turbulent fluid between $x/d = 120$ and $x/d = 192$. This process is shown in Figures 4. 29, 4. 30 and 4. 31.

4. 6 Conclusions

From the present study, the following conclusions are drawn:

1. It is possible to attain a Reynolds number of at least 6, 700 for a parabolic laminar flow in a high aspect ratio channel. This is greater than a 100 percent increase over previous investigations and it is 87 percent of the theoretical linear stability theory value of 7, 700. The transition Reynolds number can be monotonically increased by decreasing the fluctuation intensity.

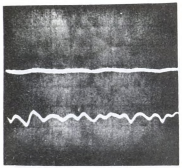

z=0

z=16½"

.5 sec./div.

Figure 4.25 Corner Effects - Laminar Flow, x=10'

Hot Wire Output Anem.

x=10', y=0, x/d=240

Rey=6,500

V. Scale 10 millivolts/div.

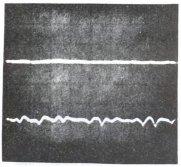

z=0

z=16½"

.5 sec./div.

Figure 4.26 Corner Effects - Laminar Flow, x=6'

Hot Wire Output Anem.

x=6', y=0, x/d=144

Rey=6,500

V. Scale 10 millivolts/div.

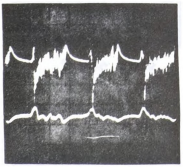

z=0

z=16½"

.5 sec./div.

Figure 4.27 Corner Effects - Bursting, x=10'

Hot Wire Output Anem.

x=10', y=0, x/d=240

Rey=7,000

V. Scale 50 millivolts/div.

Blocking Capacitor Employed

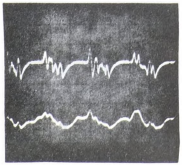

z=0

z=16½"

.5 sec./div.

Figure 4.28 Corner Effects - Bursting, x=6'

Hot Wire Output Anem.

x=6', y=0, x/d=144

Rey=7,000

V. Scale 10 millivolts/div.

Blocking Capacitor Employed

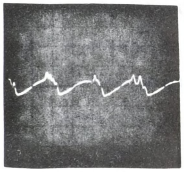

.5 sec./div.

Figure 4.29 Slug Developing, x=4'
Hot Wire Output Anem.
x=4', y=0, z=0, x/d=96
Rey=7,000
V. Scale 10 millivolts/div.

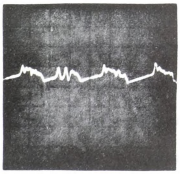

.5 sec./div.

Figure 4.30 Slug Developing, x=6'
Hot Wire Output Anem.
x=6', y=0, z=0, x/d=144
Rey=7,000
V. Scale 20 millivolts/div.

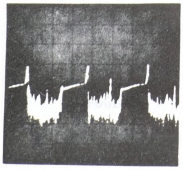

.5 sec./div.

Figure 4.31 Slug Developing, x=10'
Hot Wire Output Anem.
x=10', y=0, z=0, x/d=240
Rey=7,000
V. Scale 50 millivolts/div.

2. At Reynolds numbers slightly greater than the transition Reynolds number, the flow oscillates between a turbulent slug of fluid and a smooth laminar flow. The slug grows in size while the laminar portion of the flow decreases with increasing Reynolds numbers until the flow becomes completely turbulent. The oscillation is primarily a characteristic of the channel flow configuration.
3. As the natural transition Reynolds number is approached, there are small waves near the wall that take on a more regular shape and increase in frequency with increasing Reynolds numbers. Preceeding the first burst a near-perfect sine wave with a frequency of approximately 80 hertz is detected. This is assumed to be the Tollmein-Schlichting wave of linear stability theory.
4. The transition process remains two-dimensional as it proceeds to the turbulent burst. The burst travels with a wave front which is independent of the z-coordinate.
5. The developing flow in the entrance region is found to be more stable than a plane Poiseuille flow. At a location of $x = 1$ foot and a Reynolds number of 8,500, there exists a stable flow, as shown in Figure 4.12, even though the flow downstream is now turbulent.
6. Transition, when caused by an external excitation, results in the formation of a stability curve with a multitude of minimum points.

4.7 Recommendations

In this investigation a large positive spike in the velocity vector is observed at the beginning of each turbulent slug; however, the spikes disappear when the flow becomes fully turbulent. Further study as to the cause and details of this initial spike would be of interest.

Although the entrance region profile are more stable than a plane Poiseuille flow, it would be of value to experimentally determine the position at which the first burst occurs versus Reynolds number.

It would be advantageous to enter a vibrating ribbon into a plane Poiseuille flow at high Reynolds numbers and see if the same results, as those of Figure 4.19, are manifested.

Finally, it would be desirable to achieve laminar flow at a Reynolds number closer to 7,700 and to determine more accurately the causes of premature transition.

BIBLIOGRAPHY

BIBLIOGRAPHY

Beavers, G. S., Sparrow, E. M. and Magnuson, R. A. "Experiments on the Breakdown of Laminar Flow in a Parallel Plate Channel," Int. J. Heat Mass Transfer, 13, 809 (1970).

Beavers, G. S., Sparrow, E. M. and Magnuson, R. A. "Experiments on Hydrodynamically Developing Flow in Rectangular Ducts of Arbitrary Aspect Ratio," Int. J. Heat Mass Transfer, 13, 689 (1970).

Bradshaw, P., Stuart, J. T. and Watson, J. "Flow Stability in the Presence of Finite Initial Disturbances," AGARD Rept. 253 (1960).

Breslin, J. A. "An Experimental Investigation of Laminar-Turbulent Transition in Flow Through a Rectangular Pipe," Lehigh Univ. Technical Rep., No. 22 (1970).

Breslin, J. A. and Emrich, R. J. "Precision Measurements of Parabolic Profiles for Laminar Flow of Air Between Parallel Plates," Phys. Fluids, 10, 2289 (1967).

Chen, T. S. and Sparrow, E. M. "Stability of the Developing Laminar Flow in a Parallel-Plate Channel," J. Fluid Mech., 30, 209 (1967).

Couette, M. "Investigation on the Friction of Fluids," (French), Ann. Chem. Phys., 21, 433 (1890).

Davies, S. J. and White, C. M. "An Experimental Study of Flow of Water in Pipes of Rectangular Section," Roy. Soc. Proc., 19, 92 (1928).

Emmons, H. W. "The Laminar-Turbulent Transition in a Boundary Layer--Part I," J. Aero. Sci., 18, 490 (1951).

Hahneman, E., Freeman, J. C. and Finston, M. "Stability of Boundary Layers and of Flow in Entrance Section of a Channel," J. Aero. Sci., 493 (1948).

Kao, T. W. and Park, C. "Experimental Investigation of the Stability of Channel Flows. Part 1. Flow of a Single Liquid in a Rectangular Channel," J. Fluid Mech., 43, 145 (1970).

Laufer, J. "Investigation of Turbulent Flow in a Two-Dimensional Channel," NACA Rept., 1053 (1951).

Leite, R. J. "An Experimental Investigation of the Stability of Poiseuille Flow," J. Fluid Mech., 5, 81 (1959).

Lin, C. C. "On the Stability of Two-Dimensional Parallel Flows," Part I, II, and III, Quart. Appl. Math., 3 (1945, 1946).

Lin, C. C. The Theory of Hydrodynamic Stability. Cambridge University Press, London, (1955).

Loechrke, R. I., Markovin, M. V. and Fejer, A. A. "New Insights on Transition in Oscillating Boundary Layers," AFOSR Scientific Report, 70, 1586, TR.

Narayanan, M. A. B. and Narayana, T. "Some Studies on Transition from Laminar to Turbulent Flow in a Two-Dimensional Channel," Z. Agnew. Math. Phys., 18, 642 (1967).

Patel, V. C. and Head, M. R. "Some Observations on Skin Friction and Velocity Profiles in Fully Developed Pipe and Channel Flows," J. Fluid Mech., 38, 181 (1969).

Pekeris, C. L. and Shkoller, B. "Stability of Plane Poiseuille Flow to Periodic Disturbances of Finite Amplitude," J. Fluid Mech., 39, 611 (1970).

Prandtl, L. and Tietjens, O. G. Applied Hydro- and Aeromechanics. McGraw-Hill Book Co., Inc., New York (1934).

Reynolds, O. "An Experimental Investigation of the Circumstances which Determine Whether the Motion of Water Shall be direct or Sinous, and of the Law of Resistance in Parallel Channel," Phil. Trans. Roy. Soc., London, 174, 935 (1883).

Reynolds, W. C. and Potter, M. C. "Finite Amplitude Instability of Parallel Shear Flows," J. Fluid Mech., 27, 465 (1967).

Schlichting, H. Boundary Layer Theory. McGraw-Hill Book Co., Inc., New York (1962).

Schubauer, G. B. and Klebanoff, P. S. "Contribution on the Mechanics of Boundary Layer Transition," NACA Rept. No. 1289 (1956).

Schubauer, G. B. and Skramstad, H. K. "Laminar Boundary Layer Oscillations and Transition on a Flat Plate," NACA Rept. No. 909.

Sherlin, G. C. "Behavior of Isolated Disturbances Superimposed on Laminar Flow in a Rectangular Pipe," J. Res. N.B.S. Sec. A, Phys. and Chem., 64A, 281 (1960).

Squire, H. B. On the Stability for Three-Dimensional Disturbance of Viscous Fluid of Flow between Parallel Walls. Proc. Roy. Soc., London, A 142 (1933).

Thomas, L. H. "The Stability of Plane Poiseuille Flow," Physical Review, 4, 91 (1953).

Whan, G. A. and Rothfus, R. R. "Characteristics of Transition Flow Between Parallel Plates," A. I. Ch. E. Journal, 204 (1959).

Wygnanski, L. and Champagne, F. "On Transition in a Pipe," Boeing Scientific Research Laboratories, (1970)--To Be Published.

APPENDICES

APPENDIX A

APPARATUS AND INSTRUMENTATION

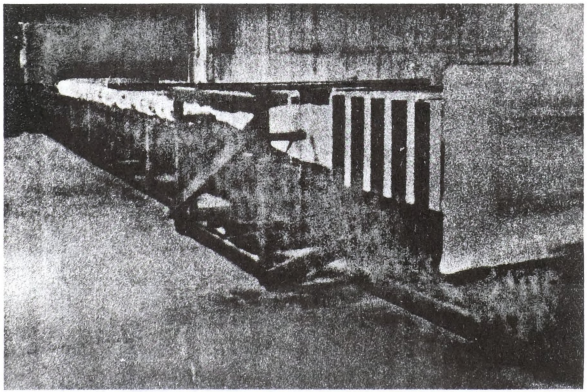

Figure A-1. Photo of channel facility.

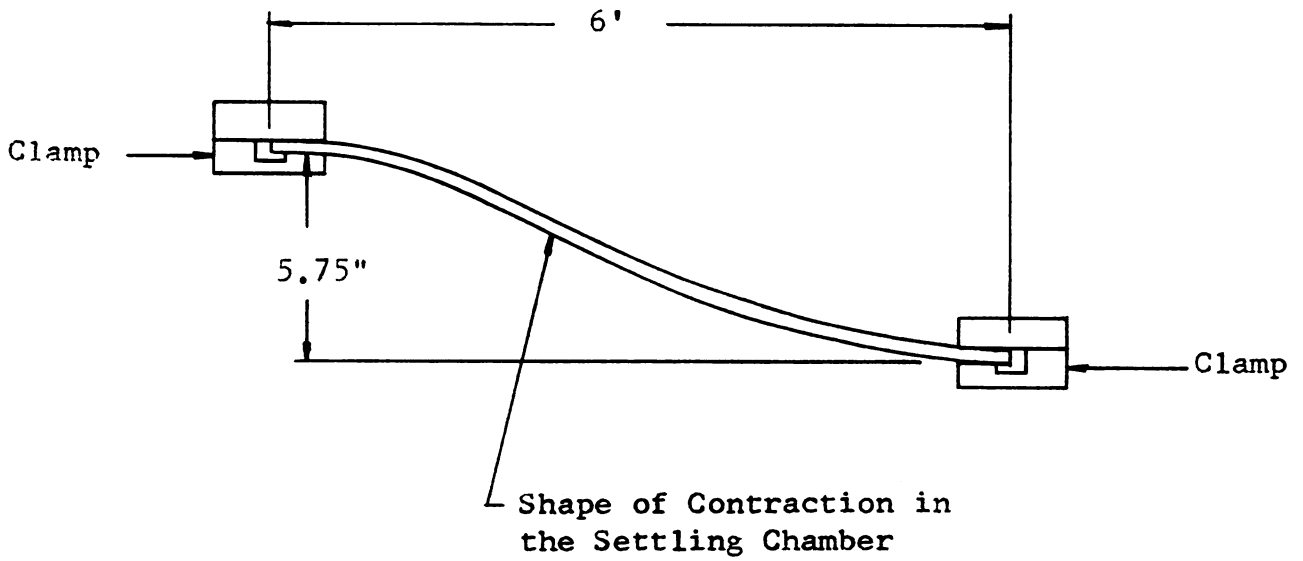

Figure A-2. Beam Deflection Curve

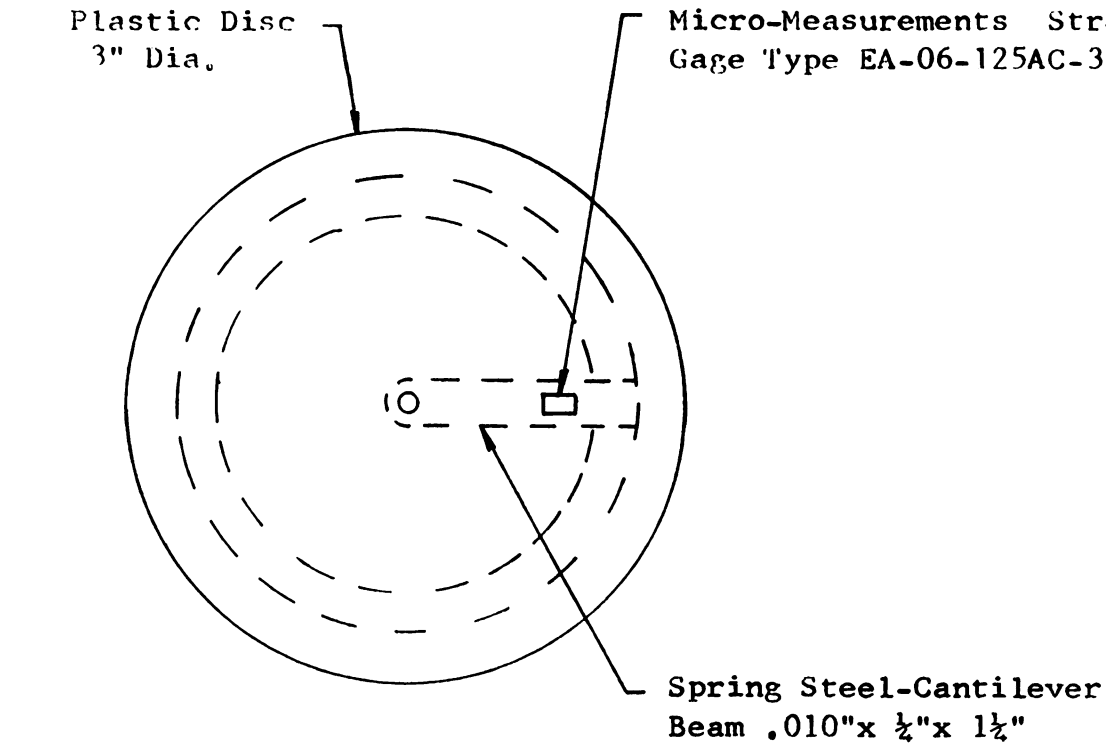

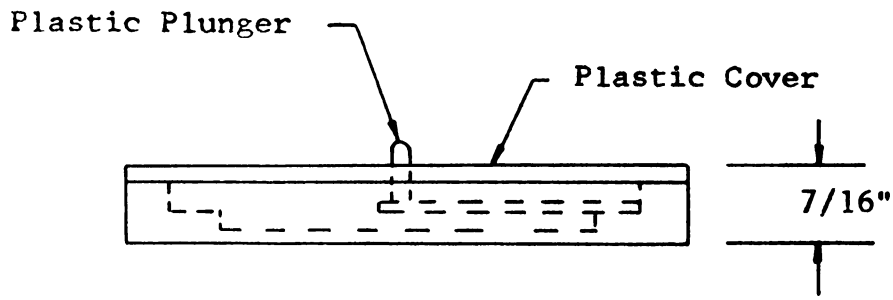

This device is calibrated outside the channel by using a micrometer.

Figure A-3. Gapping Instrument

Table A-1 Screen in the Settling Chamber

Square Mesh Screen

Mesh (per inch)	Diameter of Wire (inch.)	Open Area (%)
40	.0150	36%
80	.0055	31.4%
100	.0040	36%
120	.0037	30.7%

Table A-2 Grid Sizes Used to Increase the Velocity Fluctuation Level

Square Grid

Center to Center of Each Square (inch)	Dia. of Rods (inch)	X-Position (inch)	Transition Rey. No.
1	1/4	x = -60	6,500
2	1/2	x = -60	6,300
4	1	x = -60	5,400
1	1/4	x = -30	5,150
1½	3/8	x = -30	3,850
2	1/2	x = -30	3,300
1	1/4	x = -15	2,360
2	1/2	x = -15	2,160
4	1	x = -15	1,900

APPENDIX B

TURBULENT SLUG MODEL

The turbulent slug, described in Chapter 4, causes a variation in the average velocity of the channel. This variation in velocity oscillates with a frequency of .75 hertz, plus or minus .15 hertz. The purpose here is to calculate the average velocity as a function of time and to show why the frequency has a period of approximately 1.4 seconds. The maximum variation in average velocity is also an objective in the calculations.

It is assumed that the turbulent slug is present only in the final 16 feet of the channel and occupies only the center core of the channel width, one half of the channel width. The latter assumption is based on the observation that although the slug occurs two-dimensionally across the channel, the frequency content of the slug decreases as one approaches the corner. Figure 4.27 shows the low frequency fluctuations in the corners.

From Sherlin's study it was determined that the leading edge of the burst travels at 1.75 times the average velocity, while the trailing edge is a function of Reynolds number but is usually

close to the average velocity. Here it is assumed that the trailing edge of the slug travels at the average velocity.

At a Reynolds number of 6,950, which has an average velocity of 25 ft./sec., the leading edge of the burst travels at roughly 43 ft./sec. and the time to travel the 16 feet to the end of the channel is approximately .37 seconds. Knowing the speed of the trailing edge, the burst length is roughly 6 1/2 feet when the leading edge is exiting from the channel.

The average velocity is governed by the equation of motion in the following form:

$$\rho whL \frac{dV}{dt} = wh\Delta P - 2\tau_\ell(\tfrac{1}{2}w)L - 2\tau_\ell(\tfrac{1}{2}w)L_\ell - 2\tau_t(\tfrac{1}{2}w)L_t \qquad (B.1)$$

where,

L = 16 feet

L_ℓ is the length of the flow that is laminar

L_t is the length of the turbulent slug

$L = L_\ell + L_t$

τ_ℓ and τ_t are the laminar and turbulent shear stresses, respectively.

Now, rearranging terms and eliminating L_ℓ with $L = L_\ell + L_t$, eq. (B.1) takes on the following form:

$$\frac{dV}{dt} = \frac{\Delta P}{\rho L} - \frac{2\tau_\ell}{\rho h} + \frac{1}{\rho hL}(\tau_t - \tau_\ell)L_t \qquad (B.2)$$

The pressure in the exhaust plenum is observed to oscillate as the flow contains turbulent slugs. This is a 7 percent increase in the value of ΔP for a laminar flow. The pressure variation is shown

in Figure B-1. This variation is incorporated in eq. (B. 2) as a function of the average velocity.

The stresses are given by the following equations:

$$\tau_{\ell} = \frac{1}{2}\rho V^2 \left(\frac{12}{Rey}\right) \tag{B.3}$$

$$\tau_{t} = \frac{1}{2}\rho V^2 (.0376)\, Rey^{-\frac{1}{6}} \tag{B.4}$$

An IBM 1800 digital computer was used to integrate eq. (B. 2). The results are given in a diagram of the bursting process and a plot of the velocity, shown in Figure B-2. These relate the length of the turbulent slug and the velocity with time. The time increment of 1.5 seconds for one oscillation agrees quite well with experimental data.

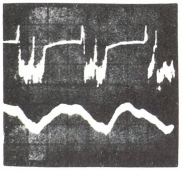

Figure B-1 Pressure Fluctuation in Exhaust Plenum

Hot Wire Anem. in Channel

Pressure Transducer in Exhaust Plenum

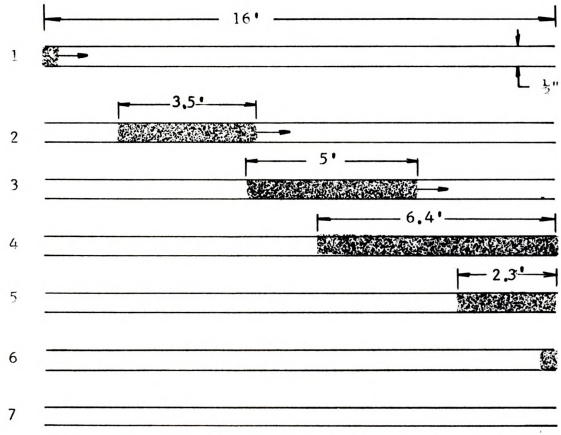

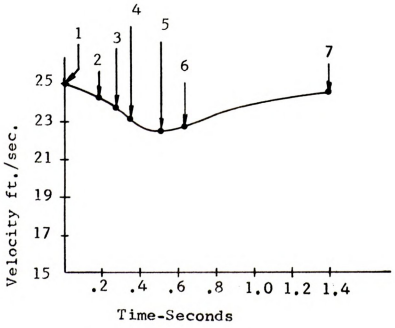

Figure B-2 Velocity Variation in the Channel